(Preprint) AAS 25-232

SPACECRAFT DYNAMICS WITH THE BACKSUBSTITUTION METHOD: SURVEY AND CAPABILITIES

João Vaz Carneiro* **and Hanspeter Schaub†**

Spacecraft simulation tools are critical to any mission design, especially early in the mission development, because they can inform whether or not the current design meets requirements. However, they are only as useful as they are accurate, which means there is a need for high-fidelity simulations that are quick to set up and fast to evaluate numerically. This requires understanding the differential equations that define the spacecraft's dynamics, which can be very complex to derive and implement. The Backsubstitution Method (BSM) is a tool used to formulate the equations of motion of spacecraft. Under the assumption that the spacecraft comprises a rigid hub to which all components attach, this approach avoids the costly inversion of the entire system mass matrix all at once. Instead, each component's accelerations can be analytically substituted directly into the hub's equations, which, after being solved numerically, can be used to solve for all other component accelerations. While the BSM has a rich history of contributions, its exact capabilities and limitations have never been thoroughly reviewed. This survey addresses this using Graph Theory, which can help describe which spacecraft configurations are allowable. This paper also thoroughly reviews all the models developed using the BSM since its inception.

INTRODUCTION

High-fidelity simulation tools are critical to any mission, particularly in the early phases of mission design, because they can help quantify whether the current design meets the mission requirements. The complexity of these tools has steadily increased to match the objectives of space missions today. Arguably, the best example is the International Space Station[1] (ISS), one of the most elaborate space vehicles ever made, composed of multiple modules assembled in orbit since its inception. The modularity to add new, more complex components is why it has accomplished its evolving science and mission objectives. Other examples include asteroid-landing missions like NASA's OSIRIS-REx[2] and JAXA's Hayabusa,[3] which require a high level of fidelity on the spacecraft's dynamics and environment effects because the forces involved are so small, meaning any small error would substantially differ from reality. Many new mission designs now propose spacecraft with intricate components that allow them to meet increasingly ambitious requirements. These can include branched elements or closed ring-like structures that can be assembled in space rather than before launch.

*Graduate Research Assistant, Ann and H.J. Smead Department of Aerospace Engineering Sciences, University of Colorado, Boulder, 431 UCB, Colorado Center for Astrodynamics Research, Boulder, CO, 80309.

†Distinguished Professor and Department Chair, Ann and H.J. Smead Department of Aerospace Engineering Sciences, University of Colorado, Boulder, 431 UCB, Colorado Center for Astrodynamics Research, Boulder, CO, 80309. AAS Fellow, AIAA Fellow.

*https://www.nasa.gov/international-space-station/

†https://science.nasa.gov/mission/osiris-rex/

‡https://www.dlr.de/en/research-and-transfer/projects-and-missions/hayabusa2/

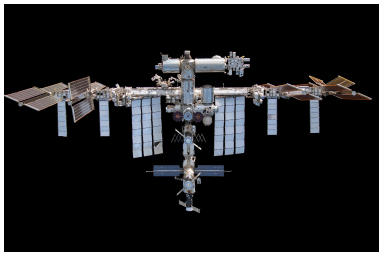

(a) ISS [*].

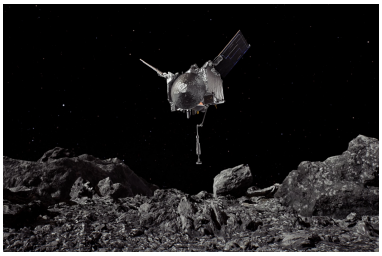

(b) OSIRIS-REx [†].

(c) Hayabusa 2 [‡].

These mission-critical features add a layer of complexity that must be included in spacecraft simulations, where the vehicle is thoroughly simulated and analyzed to ensure the spacecraft meets orbital and pointing mission requirements. These steps require the equations of motion that describe the vehicle's dynamical behavior in orbit to be derived and validated. However, simulating multi-component spacecraft is challenging due to their numerous degrees of freedom and the inherent dynamic coupling between all spacecraft components (also named effectors). Another important aspect is understanding what can and cannot be simulated under the dynamics formulation. Many formulations operate under certain assumptions that limit the spacecraft configurations that can be modeled. For example, closed-loop components may not be able to be simulated because they require numerical approximations to model the link between the two bodies that close the chain. Describing these limitations can help justify using one formulation instead of the other, depending on the use case.

Multi-body dynamics describes the motion of multiple bodies connected though differential and algebraic equations and has seen extensive study for many decades. The equations of motion can be derived using many different approaches, including force and torque-based Newtonian and Eulerian mechanics,[4] energy-based Lagrangian mechanics,[5] or Kane's Method.[6,7] Once the equations are derived, they must be rewritten in a way that solves for the states' accelerations to be numerically integrated. This can be done analytically or numerically; the former is not always possible and may require imposing constraints on the system, while the latter may be too computationally expensive. Different approaches have been proposed to avoid the computation cost of numerically solving the equations while keeping the general assumptions applicable to many systems.

Spatial Operator Algebra (SOA)[8] is an important formulation used in JPL's DARTS [§] software with many applications in robotics and aerospace. It uses spatial vectors, 6-dimensional stacked vectors of translational and rotational quantities, to define a system's mass matrix that can be inverted using an efficient recursive algorithm. NASA's 42 [¶] is a spacecraft simulation software that uses Kane's Method to formulate the equations of motion based on a tree-topology representation of the spacecraft. Each body can be rigid or flexible, and multiple bodies are connected through rotational and translational joints, although no kinematic loops are allowed. The mass matrix is inverted using a numeric algorithm such as Cholesky decomposition.[9] This work focuses on the Backsubstitution Method (BSM), used, for example, in the Basilisk [‖] framework. This formulation of spacecraft equations of motion is particularly well-suited for software implementation because of its modularity and computational speed, as shown in Reference 10. It can model spacecraft comprised of a

[§] https://dartslab.jpl.nasa.gov/

[¶] https://software.nasa.gov/software/GSC-16720-1

[‖] https://hanspeterschaub.info/basilisk/index.html

rigid hub with rigid body components attached directly, not to each other. It is well suited for how many satellites are built but has limitations in what configurations fit the formulation's assumptions.

These formulations usually have some constraints on what can and cannot be modeled, so having a tool that describes the kinematic description of the spacecraft and analyzes whether it fits the method's assumptions is very useful as the complexities of the modeled spacecraft systems increase. One tool that aids this analysis is Graph Theory.[11,12] Graph Theory studies graphs, which describe the relationship between objects, typically two at a time. Graphs have been applied to many fields, from mathematics to computer science.[13] Particularly, graphs have been used in the field of multi-body systems and robotics to describe the system's kinematic structure. Reference 14 generates the kinematic and dynamic equations of the system from its linear graph representation. Reference 15 expands this solution to the analysis of flexible multi-body systems by combining linear graph theory with the principle of virtual work. References 16–18 apply graph theory to relate the kinematic structure of the system to the analytic results and computational algorithms in multi-body dynamics using Spatial Operator Algebra. These tools can be used to analyze the structure of the spacecraft's configuration and define whether it can be modeled using the BSM.

This survey paper summarizes and contextualizes the Backsubstitution Method[19] and all its contributions to date. It thoroughly describes the method's mathematical approach to writing the equations of motion. Assuming all components attach to the hub in parallel, this formulation decouples the hub's accelerations from each component, which allows the mass matrix to be partitioned into smaller matrices (one for the hub plus one for each effector), drastically reducing the cost of inverting the system's mass matrix. To explain the applicability of the BSM, this work also explores its capabilities and limitations. This BSM formulation enables rapid spacecraft configuration prototyping and faster numerical evaluations at the cost of the challenging analytical derivation of the spacecraft component solutions, and limited configuration space. The latter is particularly important because a vehicle's kinematic structure directly impacts how it is modeled and simulated, which defines its use cases. This paper uses Graph Theory to describe the possible kinematic structure of spacecraft configurations under the Backsubstitution Method, making it possible to understand whether a particular configuration meets the criteria to be simulated with this formulation. Finally, this work extensively surveys all past contributions to the BSM, including each model's assumptions, limitations, and capabilities.

The first section introduces the mathematical description of the Backsubstitution Method and discusses its benefits and drawbacks. The second section uses Graph Theory tools to analyze the configuration space of this formulation, presenting an algorithm that can analyze the spacecraft's kinematic configuration to understand whether it can be simulated with the BSM. Finally, the third and fourth sections survey the literature on the contributions to this formulation, discussing each model while contextualizing its use cases with prior literature.

THE BACKSUBSTITUTION METHOD

Prototype Spacecraft Configuration

A prototype spacecraft configuration is shown in Figure 2. It consists of a grey rigid hub with three blue components: two flexible solar arrays and an oscillating fuel slosh particle. This general configuration is used in the following sections to describe the Backsubstitution Method approach. The hub has mass m_{hub}, center of mass location B_c and inertia about its center of mass $[I_{\text{hub},B_c}]$. The body frame $\mathcal{B} : \{\hat{\boldsymbol{b}}_1, \hat{\boldsymbol{b}}_2, \hat{\boldsymbol{b}}_3\}$ is attached to the spacecraft's hub and centered at point B. This point

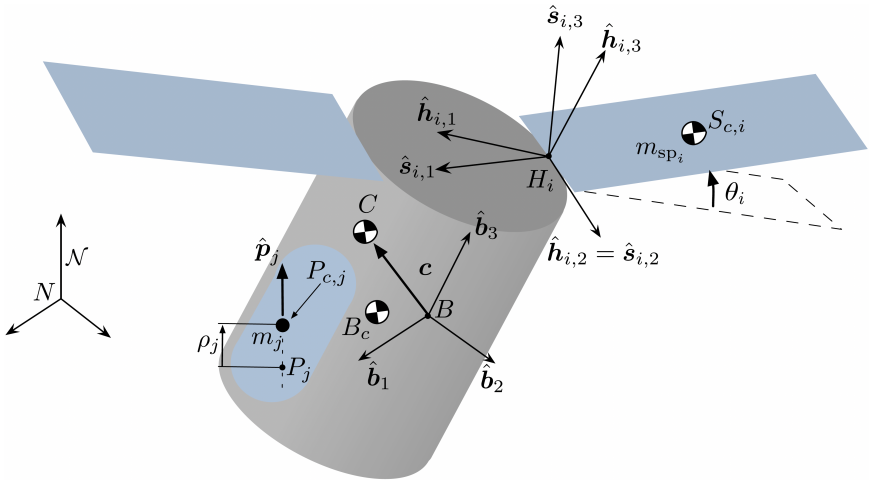

Figure 2: General spacecraft configuration.[19]

does not necessarily coincide with the hub's center of mass B_c, keeping the formulation general. Further, the body frame does not have to coincide with the hub's principal axis, which means the inertia tensor can have off-diagonal terms.

The inertial frame $\mathcal{N} : \{\hat{\boldsymbol{n}}_1, \hat{\boldsymbol{n}}_2, \hat{\boldsymbol{n}}_3\}$ is centered at point N. The hub's state variables are defined with respect to the inertial frame: the position of point B with respect to N ($\boldsymbol{r}_{B/N}$), the inertial velocity of point B with respect to N ($\dot{\boldsymbol{r}}_{B/N}$), the attitude of the $\mathcal{B}$ frame with respect to the $\mathcal{N}$ frame written in Modified Rodrigues Parameters (MRPs) ($\boldsymbol{\sigma}_{\mathcal{B}/\mathcal{N}}$), and the inertial angular velocity of the $\mathcal{B}$ frame with respect to the $\mathcal{N}$ frame ($\boldsymbol{\omega}_{\mathcal{B}/\mathcal{N}}$). While the MRP attitude set has many advantages, as described in Ref. 4, the Backsubstitution Method is agnostic to the choice of the attitude representation.

All other components have frames, mass properties, and degrees of freedom. Each of these models is also called an "effector." In Figure 2, these would be the two solar arrays and the fuel-slosh particle. For generality, each effector has mass m_{eff}, center of mass location E_c and inertia about its center of mass $[I_{\text{eff},E_c}]$. Attached to the effector is frame $\mathcal{E} : \{\hat{\boldsymbol{e}}_1, \hat{\boldsymbol{e}}_2, \hat{\boldsymbol{e}}_3\}$. Each effector is assumed to be attached directly to the hub; interconnected effectors must be modeled as a single effector with multiple degrees of freedom.

Mass Matrix Inversion

The equations of motion of mechanical systems are written in the generalized form

$$[M(\boldsymbol{q})]\ddot{\boldsymbol{q}} = \boldsymbol{f}(\boldsymbol{q}, \dot{\boldsymbol{q}}) \tag{1}$$

where $\boldsymbol{q}$ is the set of generalized states, $\dot{\boldsymbol{q}}$ is the state rate set, $\ddot{\boldsymbol{q}}$ is the state acceleration set, $[M(\boldsymbol{q})]$ is the state mass matrix and $\boldsymbol{f}(\boldsymbol{q}, \dot{\boldsymbol{q}})$ corresponds to all additional force/torque terms that do not depend directly on the state acceleration. To find the solution to the state vector through time, a direct solution to the state acceleration vector must be found, which is then numerically integrated to find the time history of the state vector. The simplest way to find the state acceleration is to invert the system mass matrix as follows

$$\ddot{\boldsymbol{q}} = [M(\boldsymbol{q})]^{-1}\boldsymbol{f}(\boldsymbol{q}, \dot{\boldsymbol{q}}) \tag{2}$$

However, inverting the system mass matrix is very computationally expensive. For an N-degree-of-freedom system, the system mass matrix has a size $N \times N$. Because a general matrix inversion algorithm has $\mathcal{O}(N^3)$ complexity, this procedure can take a long time for larger systems. Some formulations avoid the single inversion through a recursive algorithm such as SOA.[8,20] Further, the mass matrix can be fully coupled, which has implications for its software implementation.

The Backsubstitution Method (BSM) arranges the equations of motion into a specific form to avoid numerically inverting the entire system's mass matrix by making assumptions on the spacecraft configuration, allowing matrix subsets to be inverted analytically. Under the assumption that the **spacecraft comprises a rigid hub with multiple rigid bodies connected via the hub in a parallel configuration**, the system's mass matrix has a form that can be leveraged to invert smaller portions of it instead. The structure of the mass matrix under these assumptions is presented in Equation 3.

$$\begin{bmatrix} [\cdot]_{3\times3} & [\cdot]_{3\times3} & [\cdot]_{3\times N_1} & [\cdot]_{3\times N_2} & \cdots & [\cdot]_{3\times N_e} \\ [\cdot]_{3\times3} & [\cdot]_{3\times3} & [\cdot]_{3\times N_1} & [\cdot]_{3\times N_2} & \cdots & [\cdot]_{3\times N_e} \\ [\cdot]_{N_1\times3} & [\cdot]_{N_1\times3} & [\cdot]_{N_1\times N_1} & [0]_{N_1\times N_2} & \cdots & [0]_{N_1\times N_e} \\ [\cdot]_{N_2\times3} & [\cdot]_{N_2\times3} & [0]_{N_2\times N_1} & [\cdot]_{N_2\times N_2} & \cdots & [0]_{N_2\times N_e} \\ \vdots & \vdots & \vdots & \vdots & \ddots & \vdots \\ [\cdot]_{N_e\times3} & [\cdot]_{N_e\times3} & [0]_{N_e\times N_1} & [0]_{N_e\times N_2} & \cdots & [\cdot]_{N_e\times N_e} \end{bmatrix} \begin{bmatrix} \ddot{\boldsymbol{r}}_{B/N} \\ \dot{\boldsymbol{\omega}}_{\mathcal{B}/\mathcal{N}} \\ \ddot{\alpha}_1 \\ \ddot{\alpha}_2 \\ \vdots \\ \ddot{\alpha}_e \end{bmatrix} = \begin{bmatrix} [\cdot]_{3\times1} \\ [\cdot]_{3\times1} \\ [\cdot]_{N_1\times1} \\ [\cdot]_{N_2\times1} \\ \vdots \\ [\cdot]_{N_e\times1} \end{bmatrix} \tag{3}$$

The first six degrees of freedom of the state vector are the hub's position $\boldsymbol{r}_{B/N}$ and attitude $\boldsymbol{\sigma}_{\mathcal{B}/\mathcal{N}}$ (in Modified Rodrigues Parameters). All other states $\boldsymbol{\alpha}_i$ correspond to the degrees of freedom of the dynamical components directly attached to the hub. The components associated with these additional states are called **state effectors** as they contain dynamical states that need to be integrated and contribute to the system mass matrix. Each effector state set $\boldsymbol{\alpha}_i$ has N_i degrees-of-freedom. In the prototype spacecraft configuration in Figure 2, each panel has a single state θ_i, and the linearly moving mass particle has a state ρ_j. Were each panel to have two hinges, each effector state set would contain two angles.

In Eq. (3), the right-hand side contains all the terms that don't depend on the hub or effector state accelerations. These include the contributions from all state effectors and general force and torque contributions onto the hub and the effectors. A **dynamic effector** accounts for both pure force and torque space-environment contributions such as atmospheric drag and solar radiation pressure, but also contributions from thrusters or other elements that provide pure forces and torques.

Under these assumptions, the mass matrix has a unique structure. The top 6×6 matrix is fully populated and corresponds to the hub-on-hub contributions. Using the Schur complement matrix inversion method, this 6×6 hub mass matrix can be evaluated using simple numerical 3×3 inversions. The remaining terms on the first six rows and columns are also fully populated and correspond to the effector-on-hub and hub-on-effector contributions, respectively. The remaining sub-matrix can be divided into the self-effector contributions along its main block diagonal and the cross-effector terms as off-diagonal entries. Due to the centralized hub with multiple parallel effectors, all cross-effector terms are zero because the effectors do not explicitly couple with each other. This format can be leveraged to avoid inverting the entire matrix at once but instead invert smaller matrices, one for the hub and one for each additional component. Further, a key benefit is that the numerical simulation of this system can be implemented in a modular fashion. Complex spacecraft multi-body simulations are readily set up once the complex effector mathematics are resolved. There is no need to rederive the system equations of motion just because an additional panel is attached to the hub.

Rather, the multi-body spacecraft dynamics are solved in a general manner subject to the constraints of BSM.

Decoupling the effector accelerations from the hub's equations is common practice in simple components like reaction wheels.[4] For this component, the motor equation is used to remove the direct impact of the flywheel's acceleration $\dot{\Omega}$ in the hub's translational and rotational equations. This formulation is also useful for control law development. Ultimately, the BSM extends this approach to other, more complex components for its speed and modularity benefits.

Spacecraft Equations of Motion

Next, the spacecraft multi-body system equations of motion are discussed. The rigid spacecraft hub contains a set of state and dynamic effectors. As shown in Ref. 19, using the BSM, the hub's translation equations of motion are written as follows:

$$m_{\text{sc}}\ddot{\boldsymbol{r}}_{B/N} - m_{\text{sc}}[\tilde{\boldsymbol{c}}]\dot{\boldsymbol{\omega}}_{\mathcal{B}/\mathcal{N}} + \sum_{i=1}^{N_{\text{eff}}}[\boldsymbol{v}_{\text{Trans,LHS}_i}]\ddot{\alpha}_i = \boldsymbol{F}_{\text{ext}} - 2m_{\text{sc}}[\tilde{\boldsymbol{\omega}}_{\mathcal{B}/\mathcal{N}}]\boldsymbol{c}' - m_{\text{sc}}[\tilde{\boldsymbol{\omega}}_{\mathcal{B}/\mathcal{N}}][\tilde{\boldsymbol{\omega}}_{\mathcal{B}/\mathcal{N}}]\boldsymbol{c} + \sum_{i=1}^{N_{\text{eff}}}\boldsymbol{v}_{\text{Trans,RHS}_i} \quad (4)$$

As with Equation 1, all acceleration terms are multiplied by mass-like terms on the left-hand side. The right-hand side contains all force/torque-like terms that depend on zeroth or first-order terms. The equation above includes system parameters such as the spacecraft's total mass (m_{sc}), the spacecraft's center of mass with respect to point B ($\boldsymbol{c}$), and the body-frame derivative of the spacecraft's center of mass with respect to point B ($\boldsymbol{c}'$). N_{eff} is the total number of effectors and N_i corresponds to the number of degrees of freedom of the i-th effector. The term $[\boldsymbol{v}_{\text{Trans,LHS}_i}]$ is a $3 \times N_i$ matrix for the translational equation that maps the contribution of the i-th effector's second-order state derivative $\ddot{\alpha}_{ij}$ to the hubs linear acceleration, and $\boldsymbol{v}_{\text{Trans,RHS}_{ij}}$ is the i-th effector's 3×1 vector contribution to the forces on the right-hand side. The $\boldsymbol{F}_{\text{ext}}$ includes dynamic effector contributions to the net force acting on the system. Note the usual terms that appear on the differential equations of a rotating frame: Euler's force $\left(-m_{\text{sc}}[\tilde{\boldsymbol{c}}]\dot{\boldsymbol{\omega}}_{\mathcal{B}/\mathcal{N}}\right)$, Coriolis force $\left(-2m_{\text{sc}}[\tilde{\boldsymbol{\omega}}_{\mathcal{B}/\mathcal{N}}]\boldsymbol{c}'\right)$ and centrifugal force $\left(-m_{\text{sc}}[\tilde{\boldsymbol{\omega}}_{\mathcal{B}/\mathcal{N}}][\tilde{\boldsymbol{\omega}}_{\mathcal{B}/\mathcal{N}}]\boldsymbol{c}\right)$.

Using the BSM, the hub's rotational equations of motion can be generally written as follows:

$$m_{\text{sc}}[\tilde{\boldsymbol{c}}]\ddot{\boldsymbol{r}}_{B/N} + [I_{\text{sc},B}]\dot{\boldsymbol{\omega}}_{\mathcal{B}/\mathcal{N}} + \sum_{i=1}^{N_{\text{eff}}}[\boldsymbol{v}_{\text{Rot,LHS}_i}]\ddot{\boldsymbol{\alpha}}_i = \boldsymbol{L}_B - [\tilde{\boldsymbol{\omega}}_{\mathcal{B}/\mathcal{N}}][I_{\text{sc},B}]\boldsymbol{\omega}_{\mathcal{B}/\mathcal{N}} - [I'_{\text{sc},B}]\boldsymbol{\omega}_{\mathcal{B}/\mathcal{N}} + \sum_{i=1}^{N_{\text{eff}}}\boldsymbol{v}_{\text{Rot,RHS}_i} \quad (5)$$

The system's properties include the spacecraft's inertia matrix about point B ($[I_{\text{sc},B}]$) and its body-frame derivative ($[I'_{\text{sc},B}]$). The term $[\boldsymbol{v}_{\text{Rot,LHS}_i}]$ is a $3 \times N_i$ matrix for the rotational equation that maps the contributions of i-th effector's second-order state derivative $\ddot{\boldsymbol{\alpha}}_i$ to the hub's angular acceleration. The term $\boldsymbol{v}_{\text{Rot,RHS}_i}$ is the i-th effector's 3×1 vector contribution to the torques on the right-hand side that don't explicitly depend on second-order states. The term $\boldsymbol{L}_B$ contains the net torque acting on the system due to all dynamic effectors.

The equations of motion for the i-th state effector with any number of degrees of freedom are written in a general form as:

$$[\boldsymbol{M}_{\alpha_i}]\ddot{\boldsymbol{\alpha}}_i = [\boldsymbol{A}^*_{\alpha_i}]\ddot{\boldsymbol{r}}_{B/N} + [\boldsymbol{B}^*_{\alpha_i}]\dot{\boldsymbol{\omega}}_{\mathcal{B}/\mathcal{N}} + \boldsymbol{C}^*_{\alpha_i} \tag{6}$$

where $\ddot{\boldsymbol{\alpha}}_i$ is a stacked vector of all second-order states of the i-th effector. The $[\boldsymbol{M}_{\alpha_i}]$ is the mass matrix for the i-th effector, $[\boldsymbol{A}^*_{\alpha_i}]$ and $[\boldsymbol{B}^*_{\alpha_i}]$ are the matrices that multiply the hub's linear and angular accelerations, respectively, and $\boldsymbol{C}^*_{\alpha_i}$ is the vector of all remaining contributions, which includes any forces or torques applied to the effector. This equation can be rewritten to find an explicit solution to the second-order state for all effectors as follows:

$$\ddot{\boldsymbol{\alpha}}_i = [\boldsymbol{A}_{\alpha_i}]\ddot{\boldsymbol{r}}_{B/N} + [\boldsymbol{B}_{\alpha_i}]\dot{\boldsymbol{\omega}}_{\mathcal{B}/\mathcal{N}} + \boldsymbol{C}_{\alpha_i} \tag{7}$$

where the new terms are defined as

$$[\boldsymbol{A}_{\alpha_i}] = [\boldsymbol{M}_{\alpha_i}]^{-1}[\boldsymbol{A}^*_{\alpha_i}], \qquad [\boldsymbol{B}_{\alpha_i}] = [\boldsymbol{M}_{\alpha_i}]^{-1}[\boldsymbol{B}^*_{\alpha_i}], \qquad \boldsymbol{C}_{\alpha_i} = [\boldsymbol{M}_{\alpha_i}]^{-1}\boldsymbol{C}^*_{\alpha_i} \tag{8}$$

The fact that the effector's equation of motion depends directly on the hub states and not on other effectors is a direct consequence of the assumptions of the Backsubstitution Method. This can be leveraged by backsubstituting the solution to the effector second-order state in Equation 7 in the translation equation of motion (Equation 4) as follows:

$$\begin{aligned}\left[m_{\text{sc}}[I_{3\times3}] + \sum_{i=1}^{N_{\text{eff}}}[\boldsymbol{v}_{\text{Trans,LHS}_i}][\boldsymbol{A}_{\alpha_i}]\right]\ddot{\boldsymbol{r}}_{B/N} + \left[-m_{\text{sc}}[\tilde{\boldsymbol{c}}] + \sum_{i=1}^{N_{\text{eff}}}[\boldsymbol{v}_{\text{Trans,LHS}_i}][\boldsymbol{B}_{\alpha_i}]\right]\dot{\boldsymbol{\omega}}_{\mathcal{B}/\mathcal{N}} = \boldsymbol{F}_{\text{ext}} \\ - 2m_{\text{sc}}[\tilde{\boldsymbol{\omega}}_{\mathcal{B}/\mathcal{N}}]\boldsymbol{c}' - m_{\text{sc}}[\tilde{\boldsymbol{\omega}}_{\mathcal{B}/\mathcal{N}}][\tilde{\boldsymbol{\omega}}_{\mathcal{B}/\mathcal{N}}]\boldsymbol{c} + \sum_{i=1}^{N_{\text{eff}}}[\boldsymbol{v}_{\text{Trans,RHS}_i} - \boldsymbol{v}_{\text{Trans,LHS}_i}\boldsymbol{C}_{\alpha_i}]\end{aligned} \tag{9}$$

as well as the rotational equation of motion (Equation 5)

$$\begin{aligned}\left[m_{\text{sc}}[\tilde{\boldsymbol{c}}] + \sum_{i=1}^{N_{\text{eff}}}[\boldsymbol{v}_{\text{Rot,LHS}_i}][\boldsymbol{A}_{\alpha_i}]\right]\ddot{\boldsymbol{r}}_{B/N} + \left[[I_{\text{sc},B}] + \sum_{i=1}^{N_{\text{eff}}}[\boldsymbol{v}_{\text{Rot,LHS}_i}][\boldsymbol{B}_{\alpha_i}]\right]\dot{\boldsymbol{\omega}}_{\mathcal{B}/\mathcal{N}} = \boldsymbol{L}_B \\ - [\tilde{\boldsymbol{\omega}}_{\mathcal{B}/\mathcal{N}}][I_{\text{sc},B}]\boldsymbol{\omega}_{\mathcal{B}/\mathcal{N}} - [I'_{\text{sc},B}]\boldsymbol{\omega}_{\mathcal{B}/\mathcal{N}} + \sum_{i=1}^{N_{\text{eff}}}[\boldsymbol{v}_{\text{Rot,RHS}_i} - \boldsymbol{v}_{\text{Rot,LHS}_i}\boldsymbol{C}_{\alpha_i}]\end{aligned} \tag{10}$$

For a more compact notation, the following quantities are defined

$$[A] = m_{\text{sc}}[I_{3\times 3}] + \sum_{i=1}^{N_{\text{eff}}} [\boldsymbol{v}_{\text{Trans,LHS}_i}][\boldsymbol{A}_{\alpha_i}] \tag{11}$$

$$[B] = -m_{\text{sc}}[\tilde{\boldsymbol{c}}] + \sum_{i=1}^{N_{\text{eff}}} [\boldsymbol{v}_{\text{Trans,LHS}_i}][\boldsymbol{B}_{\alpha_i}] \tag{12}$$

$$[C] = m_{\text{sc}}[\tilde{\boldsymbol{c}}] + \sum_{i=1}^{N_{\text{eff}}} [\boldsymbol{v}_{\text{Rot,LHS}_i}][\boldsymbol{A}_{\alpha_i}] \tag{13}$$

$$[D] = [I_{\text{sc},B}] + \sum_{i=1}^{N_{\text{eff}}} [\boldsymbol{v}_{\text{Rot,LHS}_i}][\boldsymbol{B}_{\alpha_i}] \tag{14}$$

$$\boldsymbol{v}_{\text{Trans}} = \boldsymbol{F}_{\text{ext}} - 2m_{\text{sc}}[\tilde{\boldsymbol{\omega}}_{\mathcal{B}/\mathcal{N}}]\boldsymbol{c}' - m_{\text{sc}}[\tilde{\boldsymbol{\omega}}_{\mathcal{B}/\mathcal{N}}][\tilde{\boldsymbol{\omega}}_{\mathcal{B}/\mathcal{N}}]\boldsymbol{c} + \sum_{i=1}^{N_{\text{eff}}} [\boldsymbol{v}_{\text{Trans,RHS}_i} - \boldsymbol{v}_{\text{Trans,LHS}_i}\boldsymbol{C}_{\alpha_i}] \tag{15}$$

$$\boldsymbol{v}_{\text{Rot}} = \boldsymbol{L}_B - [\tilde{\boldsymbol{\omega}}_{\mathcal{B}/\mathcal{N}}][I_{\text{sc},B}]\boldsymbol{\omega}_{\mathcal{B}/\mathcal{N}} - [I'_{\text{sc},B}]\boldsymbol{\omega}_{\mathcal{B}/\mathcal{N}} + \sum_{i=1}^{N_{\text{eff}}} [\boldsymbol{v}_{\text{Rot,RHS}_i} - \boldsymbol{v}_{\text{Rot,LHS}_i}\boldsymbol{C}_{\alpha_i}] \tag{16}$$

which yields a compact form of the coupled translation and rotation equations of motion as

$$\begin{bmatrix} [A] & [B] \\ [C] & [D] \end{bmatrix} \begin{bmatrix} \ddot{\boldsymbol{r}}_{B/N} \\ \dot{\boldsymbol{\omega}}_{\mathcal{B}/\mathcal{N}} \end{bmatrix} = \begin{bmatrix} \boldsymbol{v}_{\text{Trans}} \\ \boldsymbol{v}_{\text{Rot}} \end{bmatrix} \tag{17}$$

The hub's accelerations can be solved using the Schur complement matrix formulation

$$\dot{\boldsymbol{\omega}}_{\mathcal{B}/\mathcal{N}} = \left([D] - [C][A]^{-1}[B]\right)^{-1} \left(\boldsymbol{v}_{\text{Rot}} - [C][A]^{-1}\boldsymbol{v}_{\text{Trans}}\right) \tag{18}$$

$$\ddot{\boldsymbol{r}}_{B/N} = [A]^{-1}\left(\boldsymbol{v}_{\text{Trans}} - [B]\dot{\boldsymbol{\omega}}_{\mathcal{B}/\mathcal{N}}\right) \tag{19}$$

The explicit hub accelerations can then be substituted into Equation 7 for each effector, which yields a solution to all second-order states. Notice how the method only requires inverting 3×3 matrices, which is computationally efficient.

Energy and Angular Momentum

A critical part of developing equations of motion is to verify that they are correct. This is done by calculating the energy and angular momentum of the spacecraft, which, when in a conservative environment and disregarding small numerical errors, are conserved throughout the simulation. These quantities are further separated into orbital energy and angular momentum *of* the hub's center of mass and rotational, orbital energy and angular momentum *about* the hub's center of mass. See Ref. 19 for the full derivation of these quantities.

The orbital energy is given by

$$T_{\text{orb}} = \frac{1}{2} m_{\text{sc}} \dot{\boldsymbol{r}}_{C/N} \cdot \dot{\boldsymbol{r}}_{C/N} \tag{20}$$

which can be simplified to use point B instead of the system's center of mass C

$$T_{\text{orb}} = \frac{1}{2} m_{\text{sc}} \left(\dot{\boldsymbol{r}}_{B/N} \cdot \dot{\boldsymbol{r}}_{B/N} + 2\dot{\boldsymbol{r}}_{B/N} \cdot \dot{\boldsymbol{c}} + \dot{\boldsymbol{c}} \cdot \dot{\boldsymbol{c}}\right) \tag{21}$$

The rotational energy is given by

$$T_{\text{rot}} = \frac{1}{2}\boldsymbol{\omega}_{\mathcal{B}/\mathcal{N}} \cdot [I_{\text{hub},B_c}]\boldsymbol{\omega}_{\mathcal{B}/\mathcal{N}} + \frac{1}{2}m_{\text{hub}}\dot{\boldsymbol{r}}_{B_c/C} \cdot \dot{\boldsymbol{r}}_{B_c/C} + \sum_{i=1}^{N_{\text{eff}}} \left(\frac{1}{2}\boldsymbol{\omega}_{\mathcal{E}_i/\mathcal{N}} \cdot [I_{\text{eff},E_{c_i}}]\boldsymbol{\omega}_{\mathcal{E}_i/\mathcal{N}} + \frac{1}{2}m_{\text{eff}}\dot{\boldsymbol{r}}_{E_{c_i}/C} \cdot \dot{\boldsymbol{r}}_{E_{c_i}/C} \right) \quad (22)$$

which can also be simplified to use point B

$$T_{\text{rot}} = \frac{1}{2}\boldsymbol{\omega}_{\mathcal{B}/\mathcal{N}} \cdot [I_{\text{hub},B_c}]\boldsymbol{\omega}_{\mathcal{B}/\mathcal{N}} + \frac{1}{2}m_{\text{hub}}\dot{\boldsymbol{r}}_{B_c/B} \cdot \dot{\boldsymbol{r}}_{B_c/B} + \sum_{i=1}^{N_{\text{eff}}} \left(\frac{1}{2}\boldsymbol{\omega}_{\mathcal{E}_i/\mathcal{N}} \cdot [I_{\text{eff},E_{c_i}}]\boldsymbol{\omega}_{\mathcal{E}_i/\mathcal{N}} + \frac{1}{2}m_{\text{eff}}\dot{\boldsymbol{r}}_{E_{c_i}/B} \cdot \dot{\boldsymbol{r}}_{E_{c_i}/B} \right) - \frac{1}{2}m_{\text{sc}}\dot{\boldsymbol{c}} \cdot \dot{\boldsymbol{c}} \quad (23)$$

The orbital angular momentum is given by

$$\boldsymbol{H}_{\text{orb},N} = m_{\text{sc}}\boldsymbol{r}_{C/N} \times \dot{\boldsymbol{r}}_{C/N} \quad (24)$$

which can be simplified to

$$\boldsymbol{H}_{\text{orb},C} = m_{\text{sc}} \left(\boldsymbol{r}_{B/N} \times \dot{\boldsymbol{r}}_{B/N} + \boldsymbol{r}_{B/N} \times \dot{\boldsymbol{c}} + \dot{\boldsymbol{c}} \cdot \dot{\boldsymbol{c}} \right) \quad (25)$$

Finally, the rotational angular momentum is

$$\boldsymbol{H}_{\text{rot},N} = [I_{\text{hub},B_c}]\boldsymbol{\omega}_{\mathcal{B}/\mathcal{N}} + m_{\text{hub}}\boldsymbol{r}_{B_c/C} \times \dot{\boldsymbol{r}}_{B_c/C} + \sum_{i=1}^{N_{\text{eff}}} \left([I_{\text{eff},E_{c_i}}]\boldsymbol{\omega}_{\mathcal{E}_i/\mathcal{N}} + m_{\text{eff}}\boldsymbol{r}_{E_{c_i}/C} \times \dot{\boldsymbol{r}}_{E_{c_i}/C} \right) \quad (26)$$

which can be simplified to be defined to use point B as

$$\boldsymbol{H}_{\text{rot},N} = [I_{\text{hub},B_c}]\boldsymbol{\omega}_{\mathcal{B}/\mathcal{N}} + m_{\text{hub}}\boldsymbol{r}_{B_c/B} \times \dot{\boldsymbol{r}}_{B_c/B} + \sum_{i=1}^{N_{\text{eff}}} \left([I_{\text{eff},E_{c_i}}]\boldsymbol{\omega}_{\mathcal{E}_i/\mathcal{N}} + m_{\text{eff}}\boldsymbol{r}_{E_{c_i}/B} \times \dot{\boldsymbol{r}}_{E_{c_i}/B} \right) - m_{\text{sc}}\boldsymbol{c} \times \dot{\boldsymbol{c}} \quad (27)$$

Capabilities and Limitations

The capabilities and limitations of the Backsubstitution Method are presented here to understand its use cases. This formulation's main advantages are speed and modularity.

Speed The key benefit of the Backsubstitution Method is that it is considerably faster than other formulations because it does not require inverting the entire mass matrix. Instead, the hub accelerations only require inverting 3×3 matrices. Any additional effector accelerations are solved by inverting their mass matrices of size equal to the number of degrees of freedom. Reference 10 shows in detail that the Backsubstitution Method can be up to 8 times faster than a generic QR decomposition method.[21] The enhanced speed of this formulation is particularly important for long simulations or Monte Carlo (MC) Analysis.[22] The latter is a popular approach to test the robustness of spacecraft design by running many simulations with changes to mass properties and initial conditions, among other variables, which stress-tests the dynamics formulation due to repeated computations.

Modularity Another important aspect of the Backsubstitution Method is its modularity. As shown in Equations 4 and 5, the effectors' contributions are included as a summation, which is a consequence of the assumption that all components are attached to the hub in parallel. Consequently, adding new components does not require rederiving the equations of motion for each specific configuration. Further, Equations 21, 23, 25 and 27 also show how testing can be parallelizable because the effectors' contributions are included in a summation. This means that there is no need to test different spacecraft configurations. Rather, each component can be tested separately to ensure its dynamics perform as expected.

Despite these advantages, the Backsubstitution Method also has limitations related to simulating different system configurations and developing the equations of motion.

Spacecraft Configuration Space The Backsubstitution Method cannot simulate certain spacecraft configurations because it assumes all components are directly attached to the hub. While many spacecraft fit this restriction, some layouts are not allowable under the BSM. For example, loops attached to the hub are prohibited. Because the contributions of the state effectors onto the hub have to be solved analytically, it is not generally possible to add effectors onto effectors in a branching configuration with the classical BSM. For example, a double-hinged panel cannot be simulated by adding a single-hinged panel onto another single-hinged panel; rather, a double-hinged component must be modeled and implemented. Further, if the spacecraft contains a robotic arm whose components branch out into multiple fingers, then a dedicated state effector specific to this configuration would need to be developed. A general force and torque-based multi-body spacecraft configuration is not feasible with the BSM. Rather, the BSM research has focused on developing general state effectors that each expand the spacecraft configuration space that can be modeled. This review discusses current research exploring ways to do limited branches for particular scenarios.

Equations of Motion Development The BSM mandates the equations of motion to be written to fit Equations 4, 5 and 6, which include all coupling terms. Finding these analytical state effector solutions and writing them in this form requires a substantial effort that is not present in other formulations. There is a trade-off between the complexity and time required to find the analytical equations of motion and the enhanced performance that the formulation enables. In many cases, this is a reasonable trade-off if the effector enables general spacecraft configuration space modeling enhancements and thus can be reused for many mission scenarios. Further, recent developments have greatly expanded the library of modeled components, increasing the likelihood that the dynamics of a specific component do not need to be rederived.

TOPOLOGY ANALYSIS ON THE BACKSUBSTITUTION METHOD

Graph Theory deals with graphs, which can efficiently represent the structure of many systems. One distinct interest is representing the kinematic configuration of a spacecraft with different components. Once transformed into a graph, many tools exist that interpret its structure according to specific rules. In particular, by transforming the spacecraft's configuration into a graph, it can be analyzed under the BSM assumptions to understand whether it can be modeled using this method. This defines the configuration space of the BSM, the set of all configurations that can be modeled using this formulation. This algorithm is efficient and can be altered as new models are introduced to the BSM.

Spacecraft Kinematic Structure with Graph Theory

A graph represents the relationships between elements in a set.[11,12] A graph contains *nodes* (or vertices) connected through *edges*. A graph is *undirected* if there is no sense of direction between two nodes. A graph can also be *weighted* if weight is added to each edge. The relationship between nodes in a graph can be expressed through an adjacency matrix, a square matrix where the ij entry is one if the i-th and j-th nodes are connected and zero otherwise. The adjacency matrix (which can also be expressed as a list) can be used to define patterns in the graph, such as loops, branches, etc. Further, there exist several exploration algorithms able to search all nodes of the graph. In particular, two main categories exist for tree graphs, which are acyclic undirected graphs: depth-first and breadth-first algorithms. The former traverses the graph by visiting all child nodes first until reaching an end (leaf) node before tracing back and visiting the sibling nodes; that is, it traverses the depth of any path before moving sideways. The latter visits all sibling nodes before moving on to the next layer of child nodes, exploring the graph by layers from the original parent node. These exploration algorithms can be used in many applications, including finding the shortest path between two nodes or finding patterns within the graph.

Graph theory is important to mechanics because it can analyze the system's configuration. In this application, the graph represents the vehicle's kinematic structure, i.e., how each body is connected. Each node corresponds to a rigid body, and each edge to a joint. The edge can be weighted to represent that joint's degrees of freedom. An example of the relationship between the kinematic structure and its graph representation is shown in Figure 3. The spacecraft consists of a rigid hub with two effectors. The first is an antenna attached to the hub by a rigid arm. The arm can rotate on one axis, and the dish can rotate about two axes. The second is a solar panel composed of three subpanels. The middle panel rotates about the hub through a one-axis joint, which moves the entire solar panel assembly, and each subpanel also rotates about the middle one via a hinge. The weighted

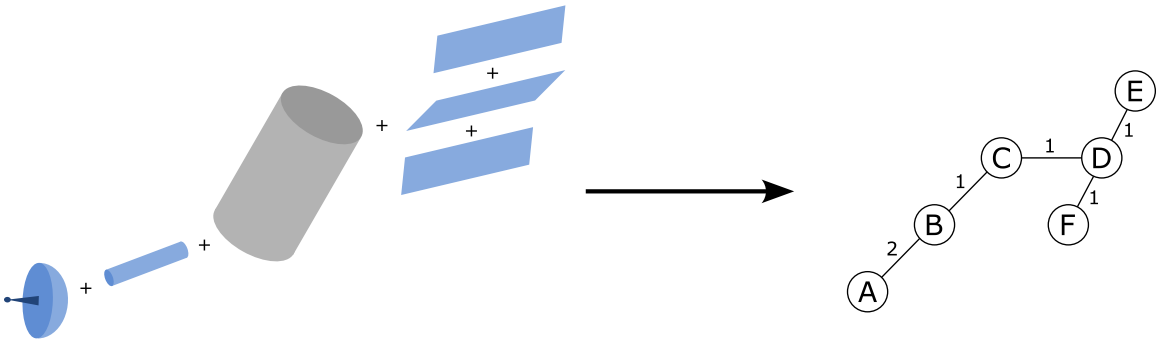

Figure 3: Interpretation of the kinematic structure of the spacecraft as an undirected graph.

undirected graph has one node for each body and one edge for each joint. Nodes A-B describe the antenna effector, where an edge with weight two connects bodies A and B, representing a two-axis joint, and an edge with weight one connects the hub and body B, depicting the one-axis hinge. Nodes D-E-F represent the solar panel assembly, each connected by an edge with a weight of one.

Application to the Backsubstitution Method

The vehicle's kinematic structure is converted into a graph and analyzed to find the spacecraft configurations that can be modeled using the classical Backsubstitution Method. Examples of spacecraft configurations using graphs are shown in Figure 4.

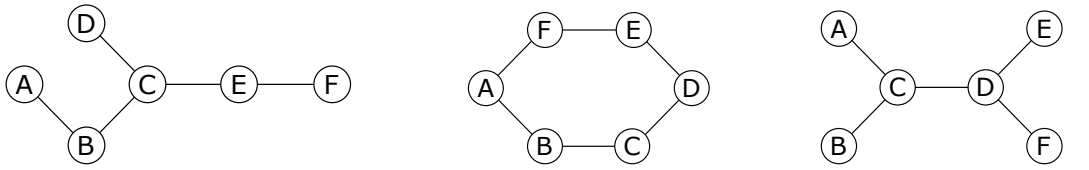

(a) Acceptable topology. (b) Unacceptable topology. (c) Unacceptable topology.

Figure 4: Examples of acceptable and unacceptable topologies.

Figure 4a is an acceptable configuration because there is only one node where multiple forks emerge. This is equivalent to a centralized hub (node C) with three effectors (A-B, D, and E-F). Figure 4b cannot be modeled using the Backsubstitution Method because closed-loop effectors imply the mass matrix is fully coupled. Finally, Figure 4c also shows an unacceptable topology because there is more than one node with forks, which means the mass matrix is populated in a way that cannot be decoupled.

The rules of the classical Backsubstitution Method can be translated into an algorithm for two purposes: to find whether the configuration can be simulated and to pick an appropriate base node. The last goal comes from the semi-arbitrary choice of which body is central. While the spacecraft's rigid hub is usually treated as the central body, the Backsubstitution Method is agnostic to which body is chosen, as long as the configuration can still be simulated. In fact, there are certain configurations where the Backsubstitution Method cannot simulate the system if the hub is picked as the central body but can model the system if another body is picked. Figure 3 is an example of this. If node C (the hub) is picked as the base, branching at node D is not allowed under the current capabilities of the BSM. However, the configuration can be simulated if node D is the base.

Figure 5 shows the search algorithm as a flowchart. The algorithm takes a depth-first approach to find whether the configuration can be simulated under the Backsubstitution Method constraints, including the models that have been developed. It explores the graph representation of the spacecraft configuration to find a suitable hub body. It works under the assumption that no closed cycles or branching are allowed. Further, it does not distinguish between rotational and translational joints. This distinction is important because only rotational or translational chains have been modeled, not mixed joints. Therefore, this algorithm must be slightly adapted until a more general translation-rotation formulation is developed. The search algorithm works as follows:

1. Pick a node as a candidate for the base node that has not been analyzed yet.
2. Check if all nodes have been analyzed. If so, no viable base has been found, and the configuration cannot be simulated for all nodes.
3. Sweep all adjacent nodes to the candidate base node. For each node, check if it has been visited. If so, the configuration has a closed cycle and cannot be simulated.
4. If the node has not been visited, check if the node has more than one edge. If so, the configuration has a branch and an invalid candidate node. Pick another candidate node.
5. Check if the current node is the end/leaf node. If not, move to the next adjacent node.
6. If it is the last node in the chain, check if all adjacent nodes have been analyzed. If not, check the other nodes. If so, the candidate to base node is picked as the base.

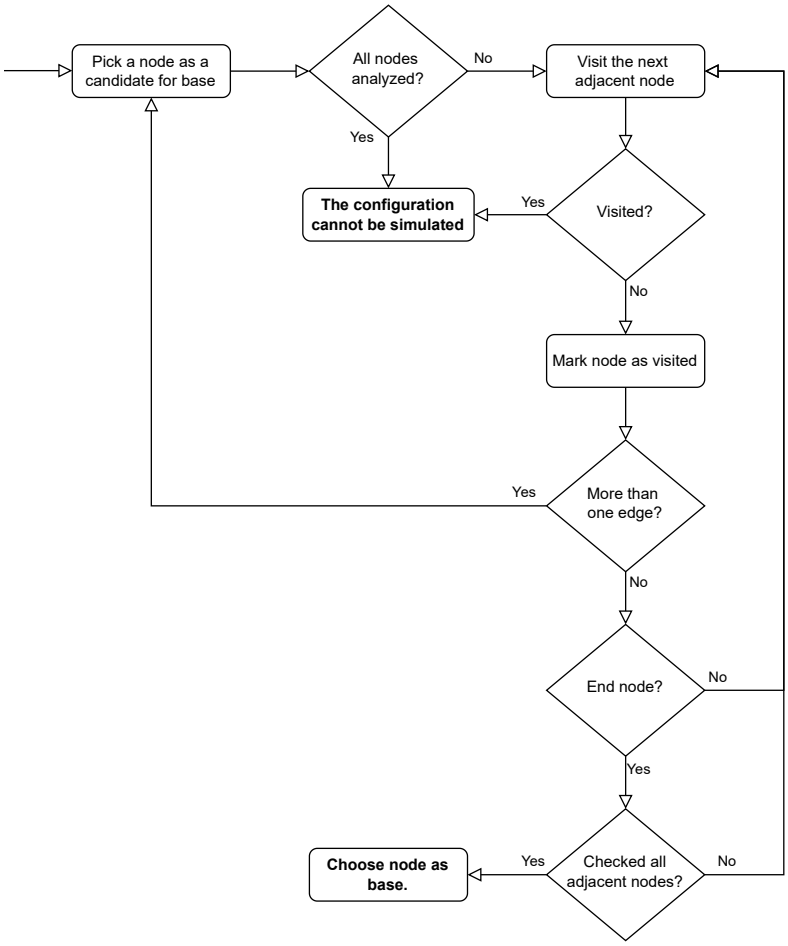

Figure 5: Search algorithm.

Note that this algorithm, as written, exits when the first viable node is found. However, a more refined algorithm could pick the base node from a pool of all viable nodes. For example, Equation 8 shows that the effector mass matrices must be inverted to solve the effector's state accelerations. Therefore, the base node can be picked to minimize any effector's maximum degrees of freedom since the inversion takes $\mathcal{O}(N^3)$ complexity.

CLASSICAL STATE EFFECTOR SOLUTIONS

State effectors are components whose motion either impacts the spacecraft's mass properties or has states to integrate. Many state effector components have been modeled using the Backsubstitution Method and developed in an increasingly general form to broaden the spacecraft configurations that can be modeled using this formulation. These are all analytic, fully coupled solutions to the spacecraft's equations of motion. This section motivates the development of different models while showcasing their use cases and assumptions.

The equations of motion may be developed for single or multiple components of the same type attached to the hub. The models with more than one component usually come as a group from the manufacturer, so the equations include a summation of each device. In any case, the equations do

not include contributions from other effectors. The resulting equations are still valid when other components are added because of the inherent modularity of the Backsubstitution Method. As discussed, the BSM accounts for all effector contributions in parallel as a summation, meaning all single-component solutions are valid in the more complex, multi-effector configuration.

Control Moment Devices

The first modeled components are control moment devices that affect the spacecraft's attitude. They are also called momentum-exchange devices because they absorb or impart the hub's angular momentum to change its angular velocity and, indirectly, its attitude. Two components are considered: reaction wheels and variable-speed control moment gyroscopes. An important challenge to using these devices is the jitter effect they can induce on the spacecraft due to mass imbalances in the flywheels.[23,24] This reaction can induce vibration in the spacecraft, potentially exciting structural modes, or hinder the operation of very precise instruments,[25] causing smear on their data. Therefore, understanding the effects of jitter through an accurate model is key for spacecraft numerical simulations.

Characterizing the effects of jitter is usually done through experimentation before flight to validate the requirements. This process allows the extraction of the imbalance parameters through empirical models.[26,27] In addition to experimental models in an integrated spacecraft, it is important to use an analytical model that can be integrated into a numerical simulation in the early phases of development. A simplified model of flywheel jitter involves modeling the imparted forces and torques on the spacecraft as external disturbances.[28,29] This model is appealing due to its computationally simple formulation and because it can be constructed directly from the manufacturer's imbalance specifications. The static imbalance force is given by[30,31]

$$\boldsymbol{F}_s = U_s \Omega^2 \hat{\boldsymbol{u}} \tag{28}$$

where U_s is the static imbalance parameter taken from the component's specification sheet, Ω is the wheel speed, and $\hat{\boldsymbol{u}}$ is a unit vector normal to the wheel spin axis, usually along the wheel's center of mass offset. The dynamic imbalance torque is given by[30,31]

$$\boldsymbol{L}_d = U_d \Omega^2 \hat{\boldsymbol{v}} \tag{29}$$

where U_d is the dynamic imbalance parameter taken from the component's specification sheet, and $\hat{\boldsymbol{v}}$ is a unit vector normal to the wheel spin axis. This approach models wheel imbalances as lumped mass parameters instead of defining a center of mass location and inertia tensor.[23] The impact of wheel jitter on flexible spacecraft dynamics has also been studied.[32,33]

Despite its benefits, the lumped-parameter model is not physically realistic because it adds an internal forcing effect as an external disturbance, which is a non-conservative effect. Therefore, the system's angular momentum is not conserved, which introduces a time-varying bias in the system's angular velocity. While this does not present a problem for analysis purposes for spacecraft with small wheel imbalances compared to the overall inertia, that is not true when the wheels are poorly balanced and the ratios are large. Significant imbalances can lead to stiff differential equations not adequately modeled using external disturbances. Further, no conservation checks can be performed, an important verification step in numeric spacecraft simulations.

The approach presented here treats the jitter disturbances as true flywheel mass imbalances rather than external disturbances. Each model makes minimal assumptions to ensure enough generality for

the user to input parameters from the manufacturer's design sheet. Therefore, momentum checks for verification purposes can be performed, as the model encompasses the fully coupled dynamics.

A reaction wheel is a disk-shaped component that rotates about a single axis $\hat{\boldsymbol{g}}_s$. Reference 34 develops the equations of motion for a set of reaction wheels using a minimal coordinate set representation for a group of single-degree-of-freedom components. The formulation is performed for a set of reaction wheels, not just one. This means the effector has a single equation of motion for $\ddot{\theta}$ for each wheel.

The problem statement is shown in Figure 6. There are two important frames associated with each reaction wheel: the mounting frame $\mathcal{M} : \{M, \hat{\boldsymbol{m}}_1, \hat{\boldsymbol{m}}_2, \hat{\boldsymbol{m}}_3\}$ and the wheel frame $\mathcal{W} : \{W, \hat{\boldsymbol{w}}_1, \hat{\boldsymbol{w}}_2, \hat{\boldsymbol{w}}_3\}$. The mounting frame has its first axis aligned with the spin axis, which can be defined in any orientation with respect to the body frame. The second axis is defined along the center of mass offset d, producing a *static imbalance*. For a balanced reaction wheel, the offset is zero, meaning the spin axis runs through the wheel's center of mass. The third axis is defined to complete a right-hand frame. The wheel frame is aligned with the mounting frame when $\theta = 0$ and rotates relative to the mounting frame about the spin axis. A *dynamic imbalance* can also be introduced if the wheel frame is not aligned with the wheel's principal frame, making the inertia matrix non-diagonal. Reference 34 goes into further detail about how the manufacturer's specifications can be appropriately translated into this model.

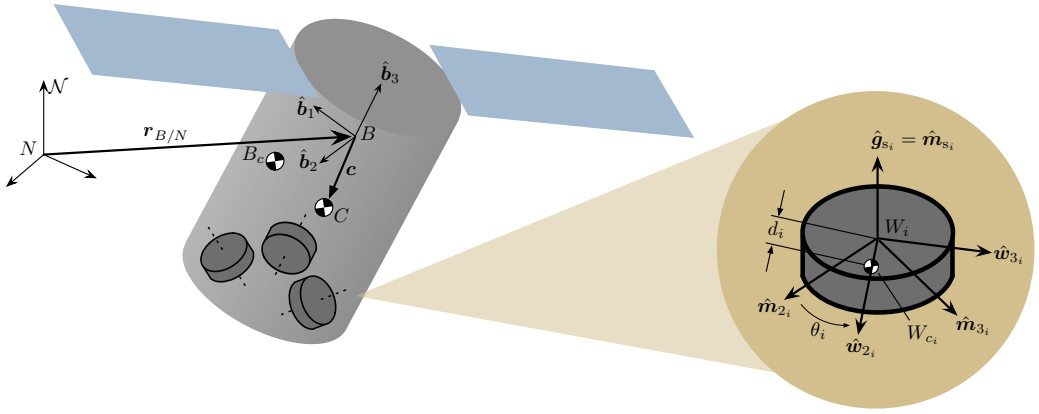

Figure 6: Reaction wheel model.[34]

The reaction wheel model makes the following assumptions:

- The spacecraft's hub is rigid, and deformations are not considered.
- The wheel's spin axis is fixed relative to the hub.
- The center of mass offset is defined perpendicular to the wheel's spin axis.

Figure 7a shows the kinematic graph representation of the reaction wheel, body B, attached to the hub, body A. In this case, the system is represented by two bodies connected through a joint with one degree of freedom since the reaction wheel rotates about a single axis. Since the equations are

written using the Backsubstitution Method, any number of reaction wheels can be attached to the hub.

(a) Reaction wheel graph. (b) VSCMG graph.

Figure 7: Kinematic graph for attitude control devices.

The dynamic model of the reaction wheel allows an external torque to be applied along the spin axis. The other axes are structural, so the spin axis does not change with respect to the body frame. The external torque can be plugged into a flight software attitude controller that maps the requested torque on the spacecraft to the available wheels, turning the component from a generic spinning body to an attitude control device, its main use case.

An important consideration for the imbalanced reaction wheel model is that it may require very small simulation timesteps. Reaction wheels spin at very high speeds, up to ten thousand rotations per minute, and any imbalance imparts a substantial gyroscopic effect on the system. Therefore, even for static or dynamic imbalances, the timestep required to maintain numeric accuracy is very small, on the order of milliseconds.

A variable-speed control moment gyroscope (VSCMG) is a two-degree-of-freedom component also used to control the spacecraft's attitude.[35,36] It consists of a disk-shaped wheel that rotates about an axis $\hat{\boldsymbol{g}}_s$ bolted to a gimbal that rotates about a perpendicular axis $\hat{\boldsymbol{g}}_g$.[4] Torques can be imposed on either axis to exchange angular momentum between the spacecraft and the VSCMG. These components can encounter singularities when controlling the spacecraft's attitude but also have a null space that can be leveraged to change their configuration without imparting any torque on the spacecraft.[4] Reference 31 derives the equations of motion of a set of variable-speed control moment gyroscopes using a minimal coordinate set with two degrees of freedom fitting the Backsubstitution Method. In this formulation, the angular velocities of each body are the main variable of interest: Ω for the wheel and $\dot{\gamma}$ for the gimbal.

As with the reaction wheel formulation, the variable-speed control moment gyroscope defines two frames. Frame $\mathcal{G} : \{G, \hat{\boldsymbol{g}}_s, \hat{\boldsymbol{g}}_t, \hat{\boldsymbol{g}}_g\}$ is attached to the gimbal such that $\hat{\boldsymbol{g}}_s$ is aligned with the wheel's spin axis, $\hat{\boldsymbol{g}}_g$ aligns with the gimbal's spin axis, and $\hat{\boldsymbol{g}}_t$ completes a right-hand frame as the second axis. The wheel frame $\mathcal{W} : \{W, \hat{\boldsymbol{w}}_1, \hat{\boldsymbol{w}}_2, \hat{\boldsymbol{w}}_3\}$ is attached to the wheel, so it rotates with it with respect to the gimbal. The first axis $\hat{\boldsymbol{w}}_1$ is defined along the spin axis, the second axis $\hat{\boldsymbol{w}}_2$ is along the wheel's center of mass offset, and the third axis $\hat{\boldsymbol{w}}_3$ completes the frame. The gimbal's center of mass G_c is general and defined as a vector with respect to G, the gimbal frame's origin. The transversal l and axial L offsets define the offset between the origins of both frames along the $\hat{\boldsymbol{g}}_s$ and $\hat{\boldsymbol{g}}_g$ axis, respectively. Finally, the wheel's center of mass offset to the wheel's frame is parameterized by d. As with the reaction wheel model, the center of mass offsets introduce imbalances to keep the formulation general.

The variable speed control moment gyroscope model makes the following assumptions:

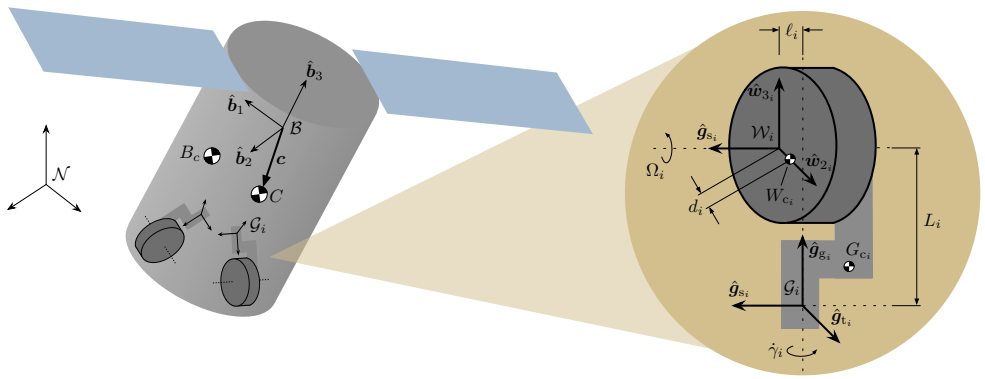

Figure 8: Variable-speed control moment gyroscope model.[31]

- The spacecraft's hub is rigid, and deformations are not considered.
- The wheel's spin axis is fixed relative to the gimbal, and and gimbal's spin axis is fixed relative to the hub.
- The center of mass offset is defined relative to the gimbal's frame.

Figure 7b shows the kinematic graph representation of the variable-speed control moment gyroscope, bodies B and C, attached to the hub, body A. In this case, the component comprises two bodies: the gimbal, B, and the flywheel, C. The effector is attached to the hub via a single-degree-of-freedom joint, which is also the case for the attachment between the wheel and the gimbal frame. Note that a chain of two individual bodies represents the component compared to the reaction wheel, which only comprises a single body rotating about a body-fixed axis.

The model allows torques to be applied at the gimbal and the wheel. VSCMGs can impart large torques on the spacecraft not by accelerating Ω like a reaction wheel but by rotating the gimbal when the wheel is spinning quickly. This takes advantage of the large gyroscopic torques from the $\dot{\gamma}\hat{\boldsymbol{g}}_g \times J_s\Omega\hat{\boldsymbol{g}}_s = J_s\Omega\dot{\gamma}\hat{\boldsymbol{g}}_t$ term along the $\hat{\boldsymbol{g}}_t$ axis, as opposed to the smaller $\dot{\Omega}\hat{\boldsymbol{g}}_s$ contribution from the wheel's acceleration. Because of this, many of these components fix the wheel speed, turning them into control moment gyroscopes. This general formulation encompasses both implementations for simpler or more complex control law applications.

As with the reaction wheels, any imbalances with high wheel speeds will produce high torques and lead to a very stiff system, necessitating a small simulation timestep to maintain numerical stability. This is even more noticeable in the VSCMG formulation because the wheel rotates with the gimbal frame, which means the torques from the imbalances change direction in the body frame as the gimbal moves.

Hinged Panels

Hinged panels are a family of components comprised of panels that rotate about a single axis. They are often used to model solar arrays stowed for launch to save space and deployed in orbit to increase surface area.[37,38] This formulation can be expanded to include a torsional spring and

damper around the hinge to approximate the first bending mode can also be used as a first-order solution to solar array flexing. While other approaches exist, this method strikes a balance between simple formulas that lack generality[39,40] and more complex formulations that require rederiving the equations of motion because the solutions are only valid for specific problems.[41–43]

Reference 44 develops the equations of motion of a spacecraft with a set of hinged panels using the Backsubstitution Method. A minimal coordinate set is used with θ being the state for each single-degree-of-freedom component. This is also the case for higher-degree-of-freedom expansions on this model.

Figure 9 shows the problem statement for the hinged panel model. The hinge frame $\mathcal{H} : \{H, \hat{\boldsymbol{h}}_1, \hat{\boldsymbol{h}}_2, \hat{\boldsymbol{h}}_3\}$ is located at the panel's hinge and perpendicular to the center of mass of the panel. The $\hat{\boldsymbol{h}}_2$ axis is coincident with the spin axis of the panel, the $\hat{\boldsymbol{h}}_1$ is defined such that, at $\theta = 0$, the panel's center of mass S has an offset d along the $-\hat{\boldsymbol{h}}_1$ direction, and $\hat{\boldsymbol{h}}_3$ completes the right-hand frame. The array frame $\mathcal{S} : \{S, \hat{\boldsymbol{s}}_1, \hat{\boldsymbol{s}}_2, \hat{\boldsymbol{s}}_3\}$ coincides with the $\mathcal{H}$ frame when $\theta = 0$, and rotates with respect to it through the $\hat{\boldsymbol{s}}_2$ axis.

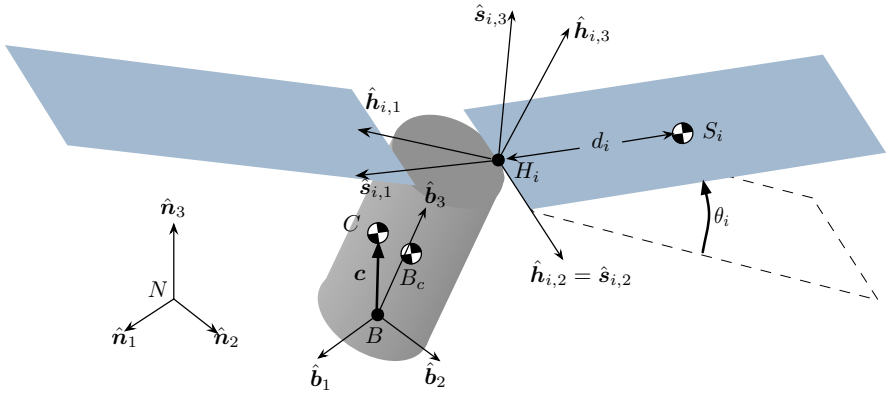

Figure 9: Single-hinged panel.[44]

The following assumptions are made when deriving the equations of motion:

- The spacecraft's hub is rigid, and deformations are not considered.
- The panel rotates about a hinge fixed relative to the hub.
- The panel and hinge frames are defined to align with the panel's spin axis and center of mass offset.

Figure 10a shows the graph representation of the kinematic structure of the single-axis panel model. It is similar to the reaction wheel's representation in Figure 7a because they share a similar formulation: one body connected to the hub through a single axis.

The array model can be used for one of two applications: panel deployment or bending frequency approximation. For the first application, a torque can be applied to the hinge axis that deploys the panel according to the intended trajectory. This requires a controller to define the required torque and a motor to apply the torque throughout the deployment. The second application includes a spring and mass damper to mimic array flexing. The spring coefficient k and damper coefficient c

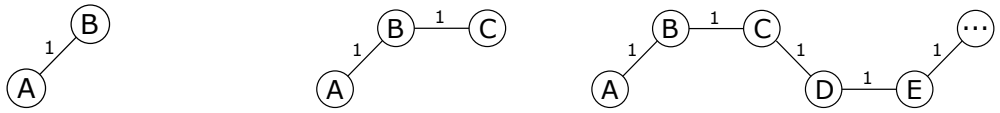

(a) Single-hinged panel graph. (b) Dual-hinged panel graph. (c) N-hinged panel graph.

Figure 10: Kinematic graph for attitude control devices.

can be defined so that the panel has a response that matches the component's natural frequency and damping ratio. Assuming a linearized response of the form $\ddot{x} + 2\zeta\omega_n\dot{x} + \omega_n^2 x = u$, the spring and mass damper coefficients are defined as follows:

$$k = I\omega_n^2, \qquad c = 2I\zeta\omega_n \tag{30}$$

where I is the bending inertia of the panel about the hinge frame, ω_n is the natural frequency, and ζ is the damping ratio.

The single-axis formulation is expanded to two degrees of freedom in Section 3.1.5 of Reference 45. The problem statement is shown in Figure 11. The dual-axis formulation is similar to the single-axis model, except now there are twice as many panel variables to define. The two panels are fully coupled, impacting each other's motion.

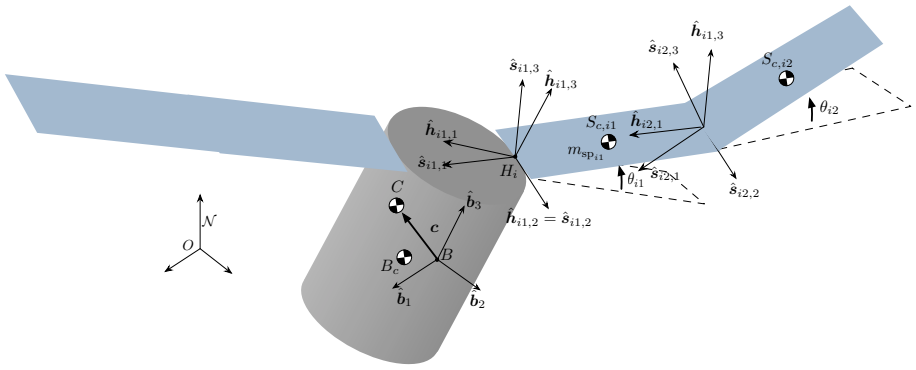

Figure 11: Dual-hinged panel.[45]

The following assumptions are made when deriving the equations of motion:

- The spacecraft's hub is rigid, and deformations are not considered.
- The first panel rotates about a hinge fixed relative to the hub, and the second fixed relative to the first.
- All hinges are parallel.
- The panel and hinge frames' are defined to align with the panels' spin axis and center of mass offset.
- Each panel's rotational motion is defined relative to the body it is connected to.

Figure 10b shows the graph for the dual-panel system. It is also similar to the VSCMG representation in Figure 7b because they are components comprised of two bodies connected through hinges. It is an expansion on the single-axis formulation to add another body. However, adding a new degree of freedom requires rederiving the equations of motion since the solution for a chain of two single-axis bodies differs greatly from the one for two one-axis bodies.

This formulation can also simulate either a two-panel deployment or two bending modes. For the former, two controllers and two motors must be simulated. For the latter, the approximation is only accurate if the two modes have very different frequencies and relative weights (also called inertia fractions). This is because the two panels cannot resonate with each other for the linearization to be valid, which implies the two frequencies cannot have similar values. Further, while the first frequency impacts the first hinge with both panels, the second frequency impacts only the second panel, which has less inertia than the two panels and, therefore, has a smaller relative weight.

Finally, the N-axis formulation is defined in Section 3.1.8 of Reference 45. It follows the same approach as the single and dual-axis formulations but expands the solution to any number of sequential panels. Figure 10c shows the graph representation of the kinematic topology of the N-axis formulation. Now, there is no limit to the number of bodies connected. However, the formulation assumes every panel is connected through parallel hinges, and no branching is allowed.

General Rotating Components

All previous solutions in References 31, 34, 44, 45 imposed some constraints on the frame, axis of motion, center of mass offset, etc. These assumptions are reasonable for the modeled component since each has geometric and functional constraints. However, the resulting equations are only valid under the assumptions made, which limits which effectors can be simulated with each model. For example, a reaction wheel and a hinged panel are rigid components that can rotate about a single axis. Therefore, their mechanics could be unified under one representation if a general single-axis spinning component was defined. The same logic can be applied to a VSCMG and a dual-hinged panel. A general formulation with fewer assumptions would help unify the dynamics under one model and expand the components that can be simulated.

The first generalization of rotating components is introduced in Reference 46 for a single-axis rotation. While this description is used to find the equations of motion of a single component attached to a hub, the Backsubstitution Method's modularity allows the solution to be used for any number of components of this type.

Figure 12 shows the problem statement for a general single-axis rotation component. The single-axis spinning body has frame $\mathcal{S} : \{S, \hat{\boldsymbol{s}}_1, \hat{\boldsymbol{s}}_2, \hat{\boldsymbol{s}}_3\}$ attached to it. The frame can have any orientation, not needing to align with the component's principal axis. This also implies a general inertia matrix $[I_{S,S_c}]$. The center of mass S_c is defined with respect to the $\mathcal{S}$ frame's origin point S and is general. Unlike previous formulations, the spin axis $\hat{\boldsymbol{s}}$ is a generic unit vector that does not have to align with any of the frame's axes.

The following assumptions are made when deriving the equations of motion:

- The spacecraft's hub is rigid, and deformations are not considered.
- The geometry and mass properties of the single degree of freedom are general.
- The properties of the single degree of freedom are defined relative to the hub.

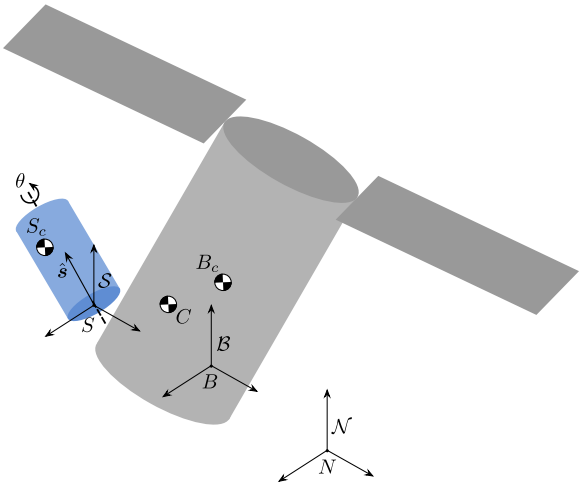

Figure 12: Single-axis rotating component diagram.[46]

- The degree of freedom θ represents translation motion about an axis fixed relative to the hub.

Developing the equations of motion for this general component requires significant effort because no assumptions are made about its geometry. Those suppositions often simplified some of the terms in the equations of motion, leading to simpler results. Without them, the development and resulting equations are more convoluted. However, this effort is justified by the enhanced configuration space that can be simulated and the unification of many models into one.

As with the hinged panel, this formulation can model a rigid body rotating about a hinge or approximate first-order flexing. It further expands that model by allowing flexing of any axis, not just bending. For example, the flexing of the torsional mode of a long cylindrical component can be modeled using this more general formulation, which cannot be modeled with the hinged panel model.

The single-axis constraint is expanded to two axes in Reference 46. An important aspect of this formulation is that it can model two single-axis bodies or one dual-axis component. If the mass and inertia associated with both degrees of freedom are non-zero, then the formulation models two bodies rotating about a hinge. If the mass properties of the lower body are set to zero, then a dual-axis effector is simulated. The upper body's mass and inertia must always be non-zero. Otherwise, the effector's mass matrix is singular and cannot be inverted to find the system's state accelerations. The ability to pick between these two components is a key benefit of this approach and would not have been possible without the lack of assumptions when deriving the equations of motion.

Figure 13 shows the problem statement for a general dual-axis rotation component. There are now two frames, $\mathcal{S}_1$ and $\mathcal{S}_2$, one for each degree of freedom. The geometry of each degree of freedom is general, with any mass, inertia, center of mass, and spin axis. The properties of the second degree of freedom are defined relative to the first.

The following assumptions are made when deriving the equations of motion:

- The spacecraft's hub is rigid, and deformations are not considered.
- The geometry and mass properties of both degrees of freedom are general.

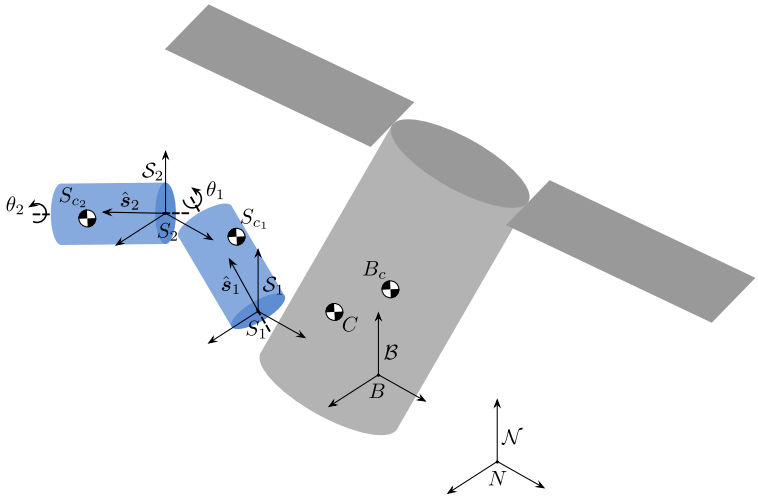

Figure 13: Dual-axis rotating component diagram.[46]

- The properties of the first degree of freedom are defined relative to the hub, and the properties of the second are relative to the first.
- The first degree of freedom represents rotational motion about an axis fixed relative to the hub and the second relative to the first.
- Each body is attached to the one before, comprising a chain with no branching allowed.

Finally, Reference 47 expands on the rotating rigid body formulation up to any number of degrees of freedom. This formulation is the full solution to a component comprised of sequentially rotating rigid links with any number of degrees of freedom. Therefore, it is a more general solution than the single and dual-axis formulations shown in Reference 46. Like the dual-axis formulation, this solution can combine multiple degrees of freedom into one link. Therefore, successive links can have up to three degrees of freedom, representing a full three-dimensional rotation between bodies. Further, this formulation can simultaneously model flexing since bending, torsional, and pinwheel modes for all links as long as the flexing motion of the component fits the sequentially linked assumption.

Figure 14 shows the problem statement for a general N-axis rotation component. Each degree of freedom has a frame $\mathcal{S}_i$, center of mass S_{c_i}, mass m_{S_i}, inertia about the center of mass $[I_{S_i,S_{c_i}}]$ and spin axis $\hat{\boldsymbol{s}}_i$. All of these properties are general and are defined with respect to body $i-1$.

- The spacecraft's hub is rigid, and deformations are not considered.
- The geometry and mass properties of each degree of freedom are general.
- The properties of each degree of freedom are always defined relative to the body upstream.
- Each degree of freedom θ_i represents rotational motion about an axis fixed relative to the upper frame.
- Each body is attached to the one before, comprising a chain with no branching allowed.

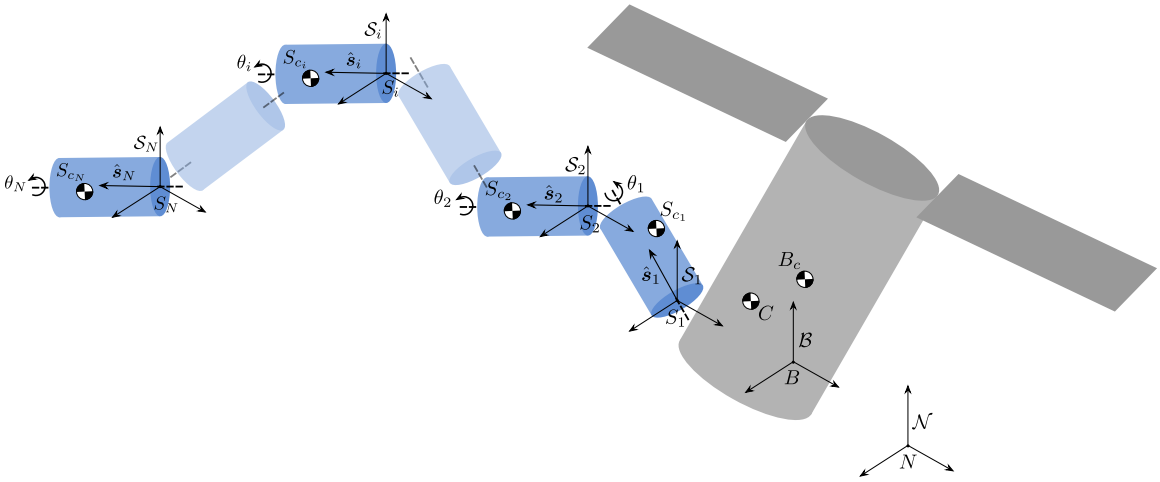

Figure 14: N-axis rotating component diagram.[47]

Figure 15 shows the kinematics graph of two components that can be modeled using this formulation. On the left, the effector comprises a chain of bodies connected through single-axis hinges. This is similar to the graph of the N-hinged panel in Figure 10c, but now there are no assumptions on the direction of the spin axis or the properties of each body. The same formulation is used on the right to model an effector where some links are connected through multi-degree-of-freedom joints. This showcases how vastly different components can be modeled under the same general formulation, assuming they comprise a chain of rotating bodies since no branching is allowed.

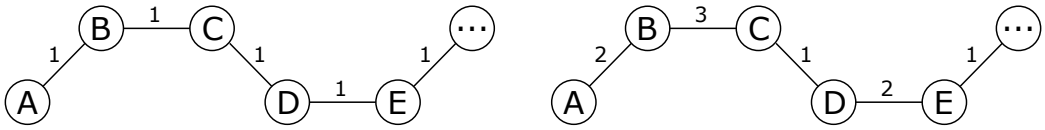

Figure 15: General N-axis spinning bodies graph.

Fuel Slosh

Fuel slosh occurs when a liquid tank is partially full, and the fuel inside can move within it. This can impact spacecraft motion, especially when the fuel comprises a significant portion of the total system's mass. This is particularly important in space where gravity acts differently than on Earth.[48,49] The Navier-Stokes equations with nonlinear boundary conditions are the highest-accuracy description for the sloshing dynamics.[45,50] Computational Fluid Dynamics (CFD) tools that numerically solve the Navier-Stokes equations have been employed to solve this problem with different formulations.[51–53] However, because of the high complexity of this phenomenon involving fluid dynamics, it is often impractical to include a fluid dynamics solution to the rigid body simulation because of its computational cost 54. Therefore, simpler models that approximate fuel slosh are introduced as first-order approximations that can be readily included in spacecraft simulation tools. These lumped mechanical multi-mode models include masses, springs, dampers, and pendulums to approximate small-amplitude waves and stable nonlinear rotary slosh.[45,54,55]

Here, two examples are introduced: the linear and pendulum slosh models. The linear model best captures the fuel's translational motion, whereas the pendulum best represents its rotational

dynamics. These models are the most accurate when the spacecraft is under constant acceleration, such as when a large burn is performed, as opposed to when the spacecraft changes attitude quickly. This is due to the complex fuel dynamics that cannot be properly captured in these simplified models except when the spacecraft's motion is simpler. Both models use a point mass assumption, meaning the fuel particle's motion does not directly impact the spacecraft's rotational motion. Instead, it indirectly impacts it through the change in the spacecraft's center of mass position and velocity caused by the fuel particle's motion.

Section 3.1.2 of Reference 45 develops the linear fuel slosh model with one degree of freedom ρ. This model is particularly effective at modeling the motion of the fuel when the spacecraft is experiencing a constant acceleration. In this case, the fuel tends to lump together on the side opposite the force's direction.

Figure 16a shows the problem statement for this model with a detail of the linear slosh effector in Figure 16b. The linear fuel slosh particle has mass m at the center of mass P_c. It moves along the $\hat{\boldsymbol{p}}$ axis with a displacement of ρ. Point P is the undeflected or equilibrium point defined to coincide with the fuel's center of mass when $\rho = 0$. Attached to the point mass is a spring with coefficient k and a damper with coefficient c. These parameters can be tuned to match the intended frequency response of the fuel slosh.

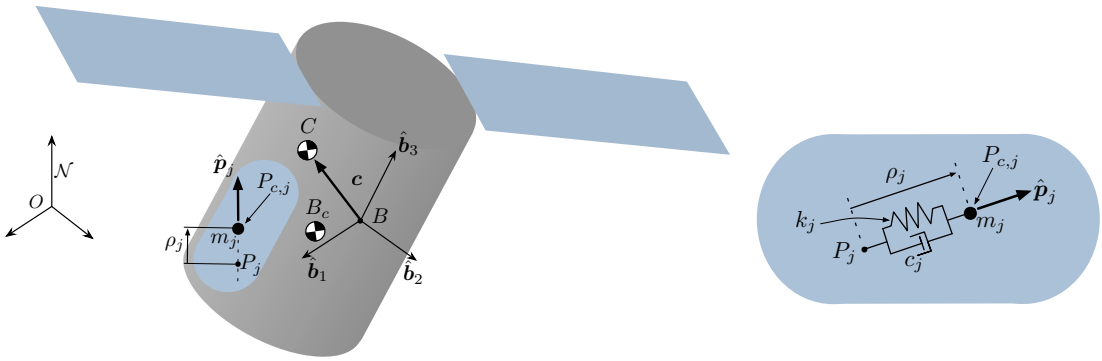

(a) Problem statement. (b) Detail.

Figure 16: Linear fuel slosh model.[45]

The linear spring-damper model has the following assumptions:

- The spacecraft's hub is rigid, and deformations are not considered.
- The fuel particle has no inertia.
- The particle can only move along a fixed direction.

Section 3.1.7 of Reference 45 develops the spherical pendulum fuel slosh model with two degrees of freedom φ and ϑ. This model is suited to model the fuel's motion under a constant rotation, oscillating sideways inside the tank.

Figure 17a shows the problem statement for this model with a detail of the pendulum slosh effector in Figure 17b. The pendulum particle has mass m at the center of mass P_c. Frame

$\mathcal{P}_0 : \{P_0, \hat{\boldsymbol{p}}_{0_1}, \hat{\boldsymbol{p}}_{0_2}, \hat{\boldsymbol{p}}_{0_3}\}$ has its origins P_0 located at the tanks geometric center. Point P is located along the $\hat{\boldsymbol{p}}_{0_1}$ axis and corresponds to the location of the point mass at equilibrium. The offset between points P_0 and P is l. Figure 17b shows the fuel particle can move freely in three-dimensional space while connected by a weightless rigid rod to the geometric center of mass of the tank. Variables φ and ϑ represent the polar and azimuth angles, respectively. φ denotes the angular displacement in the $\hat{\boldsymbol{p}}_{0_1}$-$\hat{\boldsymbol{p}}_{0_2}$ plane, while ϑ is the angular displacement out of that plane along the $\hat{\boldsymbol{p}}_{0_3}$ direction. A damper matrix D is defined to dampen the motion in all directions.

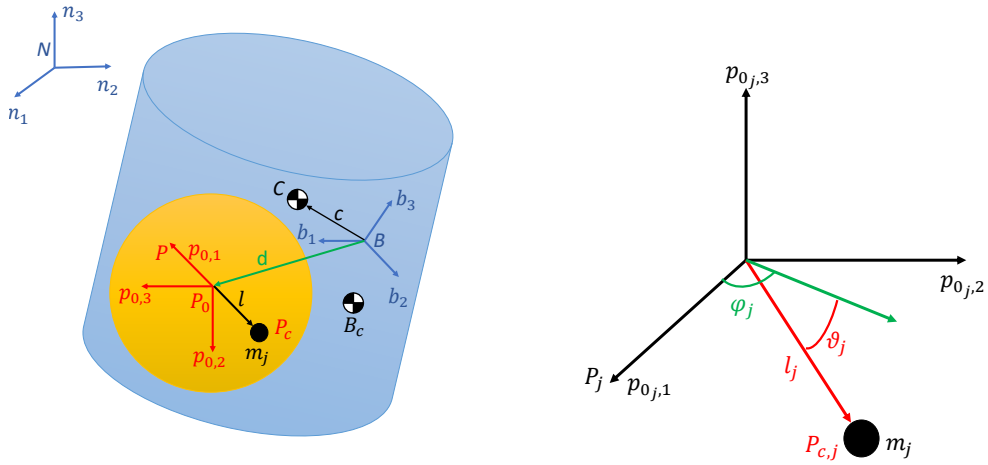

(a) Problem statement. (b) Detail.

Figure 17: Pendulum fuel slosh model.[45]

The pendulum model has the following assumptions:

- The spacecraft's hub is rigid, and deformations are not considered.
- The fuel particle has no inertia.
- The particle can move in a spherical surface with radius l.

General Translating Components

The generalization of rotating links can be extended to translating links similarly as shown in Reference 56. This is particularly important for spacecraft with robotic arms interacting physically with their environment. These include spacecraft rendezvous missions, such as Northrop Grumman's Mission Extension Vehicle[57] and the now-canceled NASA's OSAM-1[58] mission, or asteroid landers, like NASA's OSIRIS-REx mission[2] and JAXA's Hayabusa mission.[3] The interactions are often performed with a translating robotic arm with potentially multiple degrees of freedom and usually with some damping effect. Reference 56 explores the generalization of the equations of motion of a chain of translating links.

The problem statement is shown in Figure 18. Each link has two frames: $\mathcal{F}_i^0$ has point F_i^0 at its origin and is located at the body when the displacement ρ_i is equal to 0; $\mathcal{F}_i$ is located at F_i and always attached to the body. F_i is displaced from F_i^0 along the translation axis $\hat{\boldsymbol{f}}_i$ by a ρ_i

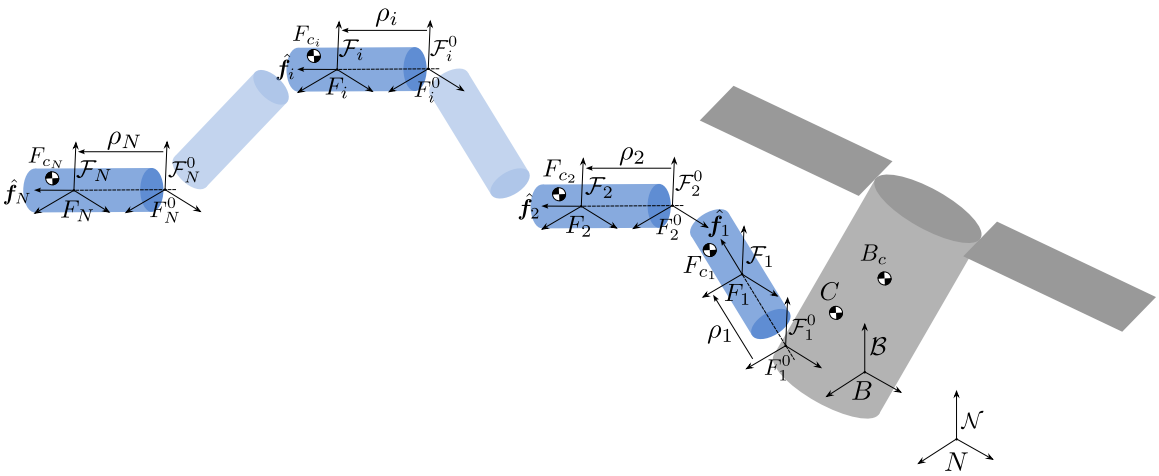

Figure 18: N-axis translating component diagram.[56]

displacement. Each degree of freedom has a center of mass F_{c_i}, mass of m_{F_i} and inertia about its center of mass $[I_{F_i,F_{c_i}}]$.

The following assumptions are made when deriving the equations of motion:

- The spacecraft's hub is rigid, and deformations are not considered.
- The geometry and mass properties of each degree of freedom are general.
- The properties of each degree of freedom are always defined relative to the body upstream.
- Each degree of freedom ρ_i represents translation motion about an axis fixed relative to the upper frame.
- Each body is attached to the one before, comprising a chain with no branching allowed.

Figure 19 shows the graph of two components comprised of sequential bodies connected through translating hinges. As with Figure 15, the joints can have more than one degree of freedom between each body. The different stroke style of the edges denotes they are translational joints, unlike the rotational joints shown before. This graph showcases the vast configuration space that the same formulation can be used to model under the assumption that no branching or closed loops exist, i.e., the effector is composed of links in a single chain.

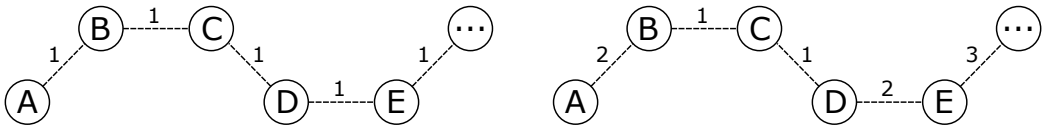

Figure 19: General N-axis translating bodies graph.

This general formulation can be used for rigid body simulations or to approximate flexing. The former can model a robotic arm with translating links, while the latter can approximate the compression of a landing strut divided into multiple sections with springs and dampers between each link. It

can also expand the linear fuel slosh particle by adding inertia, removing the point mass assumption, and including motion about more than one axis, letting the fuel move in three dimensions.

This approach can also combine multiple degrees of freedom into one body by setting the respective mass and inertia to zero. For example, if one of the links has two degrees of freedom associated with it, it can move in a plane. As with the rotational solution, the only constraint is that the last degree of freedom must have non-zero mass and inertia; otherwise, the effector's mass matrix becomes singular and non-invertible.

CLASSICAL DYNAMIC EFFECTOR SOLUTIONS

Dynamic effectors are models that impact the spacecraft's motion purely through forces and torques. These are different than state effectors, which impact the spacecraft's dynamics through their accelerations and impacts on the system's center of mass location and inertia. The contributions of the dynamic effectors are included on the right-hand side of Equations 4 and 5 in the $\boldsymbol{F}_{\text{ext}}$ and $\boldsymbol{L}_B$ terms, which represent the sum of the external forces and the external torques applied to the system, respectively. This is a key feature of the classical Backsubstitution Method: besides the impact of the state effectors, all dynamic effector contributions are applied at the system level as external effects. Therefore, even for environmental influences like drag that affect each component individually, their impact is assumed to be applied as if the spacecraft is a single rigid body.

This section presents many of the dynamic effectors developed for the Backsubstitution Method. Unlike state effectors, no equations of motion are developed because no states need to be integrated. Each model computes a force and/or torque that often depends on the spacecraft's translation or rotational states.

Device Models

The simplest dynamic effector applies a constant force and/or torque to the spacecraft, which act as external disturbances to the system. This effector can be expanded to apply pulsed forces and torques, where the duration of each pulse and between pulses can be defined. These models can be used in control applications to test control law performance and external disturbance rejection.

Magnetic torque bars,[59] also called magnetorquers, are attitude-control devices built from electromagnetic coils. They impart a torque on the spacecraft perpendicular to the magnetic field vector (often from Earth) and the magnetorquer's dipole vector. Magnetic torque bars are beneficial because they do not expend any propellant, unlike thrusters, and have no moving parts, which often leads to reliability concerns for momentum exchange devices like reaction wheels and control moment gyroscopes. However, magnetorquers also have limitations. They require large magnetic fields to produce sufficient torques, which means either a strong external field that cannot be controlled or large currents along the torque bars, which could sap a lot of energy from the spacecraft. Further, the torque produced by these devices is always perpendicular to the external magnetic field, meaning attitude cannot be controlled on all three axes.

Thruster Mass Depletion

Thrusters are components that impart thrust to a system and, depending on their location and direction, can also impart torque. In addition, thrusters expel mass out of the system, changing the physical properties of the spacecraft. The dynamics depend on the tank's relative mass property change compared to the mass ejected through the nozzle.

The most common approach to including the effect of mass ejection is an "update-only" approach, in which the spacecraft's mass, center of mass, and inertia are continuously updated as mass is expelled. While simpler to implement, this approach does not consider the dynamical influences of mass depletion on the spacecraft's motion and lacks detailed translational and rotational motion prediction. A more accurate approach involves using the Reynolds Transport Theorem,[60] which considers the spacecraft as an open system to include all the contributions from the outward mass flow. This method has been used in an axial-symmetric design with a single axial-symmetric burn chamber and a circular nozzle,[61–63] which provide a closed form solution by decoupling the rocket's axial spin from the transverse angular velocity, and in a system of two coaxial bodies[64,65] (hub with a reaction wheel), with a focus on the nutation angle of the system.

In contrast to the previous literature, the formulation in Reference 66 develops a more general set of equations of motion for a spacecraft with ejecting mass through thrusters with no assumptions on the spacecraft's geometry, tank geometry, or the complexity of the propulsion system. It writes the equations using the Backsubstitution Method, which guarantees its modularity and can be expanded to any number of thrusters. Therefore, the results can be applied to various spacecraft configurations without rederiving the equations of motion.

The contribution of this effector can be grouped as a force and torque, including the mass rate effect. Figure 20 shows the problem statement for a spacecraft comprising a hub with a thruster. The tank is in blue and located at point T_c. The geometric center of the nozzle with area A_{exh} is defined as N_c. The equations of motion aim to find the impact of accelerating mass particle M with respect to the hub frame's origin B using the Reynolds Theorem.

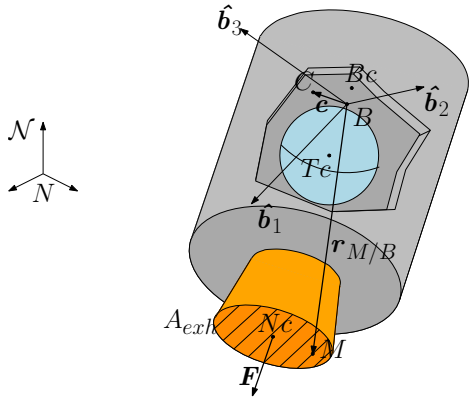

Figure 20: Thruster problem statement.[66]

The equations of motion are derived under the following assumptions:[66]

- The spacecraft's hub is rigid, and deformations are not considered.
- The mass flow among the tanks, the thrusters, and the combustion chamber are considered second-order effects and neglected. As a consequence, fluid motions in pipelines and pumps and gas whirling are not taken into account. However, the fuel expenditure related time varying fuel tank mass properties, such as total mass and inertia, are considered.
- The relative motion between the propellant and the fuel tanks, such as fuel sloshing, is not considered in this present work.

- The particles are accelerated instantaneously from the spacecraft velocity $\boldsymbol{r}_{B/N}$ to the exhausted velocity $\boldsymbol{v}_{\text{exh}}$ at the nozzle exit.
- The particle exhausted velocity $\boldsymbol{v}_{\text{exh}}$ is considered constant and parallel to the nozzle's normal $\hat{\boldsymbol{n}}$.

Environment Models

Environment models define the impact that the spacecraft experiences in different settings. For spacecraft simulations, these include disturbances from space, planets, asteroids, or other spacecraft.

Gravity is the most common environment model in spacecraft simulations. It is usually assumed to be applied at the spacecraft's center of mass and equally distributed, which is a reasonable model for many applications. An extension to this includes the addition of a gravity gradient, which results from not all spacecraft components experiencing the same gravitational force. The full solution to this torque is complex. Still, a first-order approximation can be formulated, which results in a torque along the along-track and orbit normal directions of the spacecraft's orbit.[4]

Drag is an important disturbance when the spacecraft is in low orbit, as the atmosphere's density quickly decreases with altitude. Drag always acts opposite the velocity direction. High-fidelity drag models are very complex because they numerically solve fluid dynamics equations, which depend on the spacecraft's shape and are too computationally expensive for most spacecraft simulations. Moreover, precisely knowing the density of the atmosphere is also challenging. Therefore, many simplified models of spacecraft drag exist, including the cannonball model that assumes the spacecraft is a perfect sphere.

Solar radiation pressure (SRP) is a force that acts opposite the sun's direction and mostly affects spacecraft in deep space. While its magnitude is small, it can significantly impact spacecraft around small gravitational fields around asteroids or in deep-space low-thrust missions. In both cases, the SRP is of comparable magnitude to other disturbances and cannot be ignored. Like drag, solar radiation pressure depends on the spacecraft's shape. One way to get a higher-fidelity model of SRP is to divide the spacecraft into facets and compute the resulting force at each component. While this approach is still an approximation, it is reasonably fast to compute and provides both a force and torque applied on the spacecraft. Higher-fidelity solutions include ray-tracing models[67,68] that can more precisely compute the path of the light hitting each surface on the spacecraft.

Spacecraft can charge to great voltages when interacting with plasma and the sun. This charging can create forces and torques on both objects when interacting with debris or other spacecraft. This is particularly important in active debris removal (ADR) or on-orbit servicing, assembly, and manufacturing (OSAM) missions because they involve spacecraft near each other. The interactions between spacecraft can be very complex because different components of the spacecraft may charge to different voltages. Therefore, a high-fidelity model of these forces and torques is impractical in spacecraft simulations. The multi-sphere method[69] is an approximate method that models the heterogeneous charge of the spacecraft as a series of charged spheres along its surface. This method yields fast numerical evaluations of the forces and torques produced from the interaction between charged spacecraft and is suitable for fast spacecraft simulations.

CONCLUSION

This survey paper provides an extensive overview of the Backsubstitution Method in context with other formulations to define the spacecraft's equations of motion. It reviews the mathematical ap-

proach to the BSM and how the rigid hub with parallel components assumption can be used to avoid inverting the entire system's mass matrix. The method's capabilities (speed and modularity) and limitations (configuration space and analytic complexity) are also thoroughly discussed. On that note, the spacecraft's kinematic configuration is represented using graphs, which allows a search algorithm to analyze whether the spacecraft's structure can be modeled using this formulation. Finally, a comprehensive survey of the state and dynamic effectors modeled using the Backsubstitution Method is provided.

REFERENCES

[1] L. J. DeLucas, "International Space Station," *Acta Astronautica*, Vol. 38, No. 4-8, 1996, pp. 613–619.

[2] K. Berry, B. Sutter, A. May, K. Williams, B. W. Barbee, M. Beckman, and B. Williams, "OSIRIS-REx Touch-and-go (TAG) Mission Design and Analysis," *36th Annual AAS Guidance and Control Conference*, No. GSFC. CP. 7566.2013, 2013.

[3] J. Kawaguchi, A. Fujiwara, and T. Uesugi, "Hayabusa — Its Technology and Science Accomplishment Summary and Hayabusa-2," *Acta Astronautica*, Vol. 62, No. 10-11, 2008, pp. 639–647.

[4] H. Schaub and J. L. Junkins, *Analytical Mechanics of Space Systems*. Reston, VA: AIAA Education Series, 4th ed., 2018, 10.2514/4.105210.

[5] M. Géradin and D. J. Rixen, *Mechanical vibrations: theory and application to structural dynamics*. John Wiley & Sons, 2014.

[6] T. R. Kane and D. A. Levinson, *Dynamics, theory and applications*. McGraw Hill, 1985.

[7] C. M. Roithmayr and D. H. Hodges, "Dynamics: theory and application of Kane's method," 2016.

[8] A. Jain, *Robot and Multibody Dynamics: Analysis and Algorithms*. Springer Science & Business Media, 2010.

[9] A. Krishnamoorthy and D. Menon, "Matrix Inversion Using Cholesky Decomposition," *2013 signal processing: Algorithms, architectures, arrangements, and applications (SPA)*, IEEE, 2013, pp. 70–72.

[10] C. Allard, M. Diaz-Ramos, and H. Schaub, "Computational Performance of Complex Spacecraft Simulations Using Back-Substitution," *Journal Of Aerospace Information Systems*, Vol. 16, Oct. 2019, pp. 427–436, 10.2514/1.I010713.

[11] D. B. West *et al.*, *Introduction to Graph Theory*, Vol. 2. Prentice hall Upper Saddle River, 2001.

[12] B. Bollobás, *Modern Graph Theory*, Vol. 184. Springer Science & Business Media, 2013.

[13] J. L. Gross, J. Yellen, and M. Anderson, *Graph Theory and Its Applications*. Chapman and Hall/CRC, 2018.

[14] J. J. McPhee, "On the Use of Linear Graph Theory in Multibody System Dynamics," *Nonlinear Dynamics*, Vol. 9, 1996, pp. 73–90.

[15] P. Shi and J. McPhee, "Dynamics of Flexible Multibody Systems Using Virtual Work and Linear Graph Theory," *Multibody System Dynamics*, Vol. 4, 2000, pp. 355–381.

[16] A. Jain, "Graph Theory Roots of Spatial Operators for Kinematics and Dynamics," *2010 IEEE International Conference on Robotics and Automation*, IEEE, 2010, pp. 2745–2750.

[17] A. Jain, "Graph Theoretic Foundations of Multibody Dynamics: Part I: Structural Properties," *Multibody system dynamics*, Vol. 26, 2011, pp. 307–333.

[18] A. Jain, "Graph Theoretic Foundations of Multibody Dynamics: Part II: Analysis and Algorithms," *Multibody system dynamics*, Vol. 26, 2011, pp. 335–365.

[19] C. Allard, M. Diaz-Ramos, P. W. Kenneally, H. Schaub, and S. Piggott, "Modular Software Architecture for Fully-Coupled Spacecraft Simulations," *Journal of Aerospace Information Systems*, Vol. 15, No. 12, 2018, pp. 670–683, 10.2514/1.I010653.

[20] G. Rodriguez, A. Jain, and K. Kreutz-Delgado, "A Spatial Operator Algebra for Manipulator Modeling and Control," *The International Journal of Robotics Research*, Vol. 10, No. 4, 1991, pp. 371–381.

[21] W. Gander, "Algorithms for the QR Decomposition," *Res. Rep*, Vol. 80, No. 02, 1980, pp. 1251–1268.

[22] R. Y. Rubinstein and D. P. Kroese, *Simulation and the Monte Carlo Method*. John Wiley & Sons, 2016.

[23] F. L. Markley, J. L. Crassidis, F. L. Markley, and J. L. Crassidis, *Fundamentals of Spacecraft Attitude Determination and Control*. Springer, 2014.

[24] J. R. Wertz, W. J. Larson, D. Kirkpatrick, and D. Klungle, *Space Mission Analysis and Design*, Vol. 8. Springer, 1999.

[25] L. Dewell, N. Pedreiro, C. Blaurock, K.-C. Liu, J. Alexander, and M. Levine, "Precision Telescope Pointing and Spacecraft Vibration Isolation for the Terrestrial Planet Finder Coronagraph," *UV/Optical/IR Space Telescopes: Innovative Technologies and Concepts II*, Vol. 5899, SPIE, 2005, pp. 13–26.

[26] R. Masterson, D. Miller, and R. Grogan, "Development of Empirical and Analytical Reaction Wheel Disturbance Models," *40th Structures, Structural Dynamics, and Materials Conference and Exhibit*, 1999, p. 1204.

[27] R. A. Masterson, D. W. Miller, and R. L. Grogan, "Development and Validation of Reaction Wheel Disturbance Models: Empirical Model," *Journal of sound and vibration*, Vol. 249, No. 3, 2002, pp. 575–598.

[28] L. Liu, "Jitter and Basic Requirements of the Reaction Wheel Assembly in the Attitude Control System," *Massachusetts Institute of Technology*, 2007.

[29] H. L. Gutierrez, *Performance Assessment and Enhancement of Precision Controlled Structures During Conceptual Design*. PhD thesis, Massachusetts Institute of Technology, 1999.

[30] D. Li, X. Chen, and B. Wu, "Analysis of Reaction Wheels Imbalance Torque Effects on Satellite Attitude Control System," *2016 Chinese Control and Decision Conference (CCDC)*, IEEE, 2016, pp. 3722–3725.

[31] J. Alcorn, C. Allard, and H. Schaub, "Fully-Coupled Dynamical Jitter Modeling Of Variable-Speed Control Moment Gyroscopes," *AAS/AIAA Astrodynamics Specialist Conference*, Stevenson, WA, 08 2017, pp. 1–11.

[32] K.-C. Liu, P. Maghami, and C. Blaurock, "Reaction Wheel Disturbance Modeling, Jitter Analysis, and Validation Tests for Solar Dynamics Observatory," *AIAA Guidance, Navigation and Control Conference and Exhibit*, 2008, p. 7232.

[33] D.-K. Kim, "Micro-Vibration Model and Parameter Estimation Method of a Reaction Wheel Assembly," *Journal of Sound and Vibration*, Vol. 333, No. 18, 2014, pp. 4214–4231.

[34] J. Alcorn, C. Allard, and H. Schaub, "Fully Coupled Reaction Wheel Static and Dynamic Imbalance for Spacecraft Jitter Modeling," *AIAA Journal of Guidance, Control, and Dynamics*, Vol. 41, No. 6, 2018, pp. 1380–1388, 10.2514/1.G003277.

[35] H. Schaub, S. R.Vadali, and J. L. Junkins, "Feedback Control Law for Variable Speed Control Moment Gyroscopes," *AAS Journal of the Astronautical Sciences*, Vol. 45, July–Sept. 1998, pp. 307–328.

[36] H. Schaub and J. L. Junkins, "Singularity Avoidance Using Null Motion and Variable-Speed Control Moment Gyros," *AIAA Journal of Guidance, Control and Dynamics*, Vol. 23, Jan.–Feb. 2000, pp. 11–16, 10.2514/2.4514.

[37] J. Kuang, P. A. Meehan, A. Leung, and S. Tan, "Nonlinear Dynamics of a Satellite with Deployable Solar Panel Arrays," *International Journal of Non-Linear Mechanics*, Vol. 39, No. 7, 2004, pp. 1161–1179.

[38] B. Wie, N. Furumoto, A. Banerjee, and P. Barba, "Modeling and Simulation of Spacecraft Solar Array Deployment," *Journal of Guidance, Control, and Dynamics*, Vol. 9, No. 5, 1986, pp. 593–598.

[39] M. J. Sidi, *Spacecraft Dynamics and Control: a Practical Engineering Approach*, Vol. 7. Cambridge university press, 1997.

[40] V. S. Aslanov and V. V. Yudintsev, "Dynamics, Analytical Solutions and Choice of Parameters for Towed Space Debris with Flexible Appendages," *Advances in Space Research*, Vol. 55, No. 2, 2015, pp. 660–667.

[41] G. E. Fleischer and P. W. Likins, "Attitude Dynamics Simulation Subroutines for Systems of Hinge-Connected Rigid Bodies," tech. rep., NASA, 1974.

[42] P. W. Likins, "Point-Connected Rigid Bodies in a Topological Tree," *Celestial mechanics*, Vol. 11, No. 3, 1975, pp. 301–317.

[43] W. W. Hooker, "A Set of r Dynamical Attitude Equations for an Arbitrary N-body Satellite Having r Rotational Degrees of Freedom," *AIAA Journal*, Vol. 8, No. 7, 1970, pp. 1205–1207.

[44] C. Allard, H. Schaub, and S. Piggott, "General Hinged Solar Panel Dynamics Approximating First-Order Spacecraft Flexing," *AIAA Journal of Spacecraft and Rockets*, Vol. 55, No. 5, 2018, pp. 1290–1298, 10.2514/1.A34125.

[45] C. Allard, *Modular Software Architecture for Complex Multi-Body Fully-Coupled Spacecraft Dynamics*. PhD thesis, Aerospace Engineering Sciences Department, University of Colorado, Boulder, CO, 2018.

[46] J. Vaz Carneiro, C. Allard, and H. Schaub, "General Dynamics for Single and Dual-Axis Rotating Rigid Spacecraft Components," *Journal of Spacecraft and Rockets*, Vol. 61, July–August 2024, pp. 1099–1113, 10.2514/1.A35865.

[47] J. Vaz Carneiro, C. Allard, and H. Schaub, "Rotating Rigid Body Dynamics Architecture For Spacecraft Simulation Software Implementation," *AAS Guidance and Control Conference*, Breckenridge, CO, Feb. 2–8 2023. Paper No. AAS-23-112.

[48] H. N. Abramson, "The Dynamic Behavior of Liquids in Moving Containers, with Applications to Space Vehicle Technology," tech. rep., NASA, 1966.

[49] F. T. Dodge *et al.*, "The New "Dynamic Behavior of Liquids in Moving Containers"," tech. rep., Southwest Research Institute. San Antonio, TX, 2000.

[50] J. Vreeburg and A. Veldman, "Transient and Sloshing Motions in an Unsupported Container," *Physics of fluids in microgravity*, 2002, pp. 293–321.

[51] R. Hung, Y. Long, and Y. Chi, "Slosh Dynamics Coupled with Spacecraft Attitude Dynamics. I - Formulation and Theory," *Journal of Spacecraft and Rockets*, Vol. 33, No. 4, 1996, pp. 575–581.

[52] R. Hung, Y. Long, and Y. Chi, "Slosh Dynamics Coupled with Spacecraft Attitude Dynamics. II - Orbital Environment Application," *Journal of spacecraft and rockets*, Vol. 33, No. 4, 1996, pp. 582–593.

[53] B. Marsell, S. Gangadharan, Y. Chatman, J. Sudermann, K. Schlee, and J. Ristow, "A CFD Approach to Modeling Spacecraft Fuel Slosh," *47th AIAA Aerospace Sciences Meeting including the New Horizons Forum and Aerospace Exposition*, 2009, p. 366.

[54] K. Schlee, S. Gangadharan, J. Ristow, C. Hubert, J. Sudermann, and C. Walker, "Modeling and Parameter Estimation of Spacecraft Fuel Slosh Mode," *Proceedings of the Winter Simulation Conference, 2005.*, IEEE, 2005, pp. 10–pp.

[55] D. D. Kana, "A Model for Nonlinear Rotary Slosh in Propellant Tanks," *Journal of Spacecraft and Rockets*, Vol. 24, No. 2, 1987, pp. 169–177.

[56] J. Vaz Carneiro, P. Johnson, and H. Schaub, "Backsubstitution Method For Spacecraft With Generally Translating Appendages," *AAS Astrodynamics Specialist Conference*, Broomfield, CO, Aug. 11–15 2024. Paper No. AAS 24-248.

[57] N. T. Redd, "Bringing Satellites Back from THE DEAD: Mission Extension Vehicles Give Defunct Spacecraft a New Lease on Life," *IEEE Spectrum*, Vol. 57, 2020, pp. 6–7.

[58] M. A. Shoemaker, M. Vavrina, D. E. Gaylor, R. Mcintosh, M. Volle, and J. Jacobsohn, "OSAM-1 Decommissioning Orbit Design," *AAS/AIAA Astrodynamics Specialis t Conference*, 2020.

[59] P. Wang and Y. B. Shtessel, "Satellite Attitude Control Using Only Magnetorquers," *Proceedings of the 1998 American Control Conference. ACC (IEEE Cat. No. 98CH36207)*, Vol. 1, IEEE, 1998, pp. 222–226.

[60] P. K. Kundu, I. M. Cohen, D. R. Dowling, and J. Capecelatro, *Fluid Mechanics*. Elsevier, 2024.

[61] F. Eke, T. Tran, and J. Sookgaew, "Dynamics of a Spinning Rocket with Internal Mass Flow," *Nonlinear Dynamics and Systems Theory*, Vol. 6, No. 2, 2006, pp. 129–142.

[62] F. O. Eke and T. Mao, "On the Dynamics of Variable Mass Systems," *International Journal of Mechanical Engineering Education*, Vol. 30, No. 2, 2002, pp. 123–137.

[63] J. Sookgaew and F. Eke, "Effects of Substantial Mass Loss on the Attitude Motions of a Rocket-type Variable Mass System," *Nonlinear Dynamics and Systems Theory*, Vol. 4, No. 1, 2004, pp. 73–88.

[64] V. Aslanov and A. Doroshin, "The Motion of a System of Coaxial Bodies of Variable Mass," *Journal of Applied Mathematics and Mechanics*, Vol. 68, No. 6, 2004, pp. 899–908.

[65] A. V. Doroshin, "Analysis of Attitude Motion Evolutions of Variable Mass Gyrostats and Coaxial Rigid Bodies System," *International Journal of Non-Linear Mechanics*, Vol. 45, No. 2, 2010, pp. 193–205.

[66] P. Panicucci, C. Allard, and H. Schaub, "Spacecraft Dynamics Employing a General Multi-Tank and Multi-Thruster Mass Depletion Formulation," *Journal of Astronautical Sciences*, Vol. 65, No. 4, 2018, pp. 423–447, 10.1007/s40295-018-0133-0.

[67] P. W. Kenneally and H. Schaub, "Fast Spacecraft Solar Radiation Pressure Modeling by Ray Tracing on Graphics Processing Unit," *Advances in Space Research*, Vol. 65, April 2020, pp. 1951–1964, 10.1016/j.asr.2019.12.028.

[68] P. W. Kenneally, H. Schaub, and S. Tanygin, "OpenGL-OpenCL Solar Radiation Pressure Modeling with Time-Varying Spacecraft Geometries," *AIAA Journal of Aerospace Information Systems*, Vol. 18, May 2021, pp. 307–321, 10.2514/1.I010869.

[69] J. Hughes and H. Schaub, "Heterogeneous Surface Multi-Sphere Models using Method of Moments Foundations," *Journal of Spacecraft and Rockets*, Vol. 56, August 2019, pp. 1259–1266, 10.2514/1.A34434.